Teichoic acids in the periplasm and cell envelope of *Streptococcus pneumoniae*

Mai Nguyen[a#], Elda Bauda[a#], Célia Boyat[a], Cédric Laguri[a], Céline Freton[a], Anne Chouquet[a], Benoit Gallet[a], Morgane Baudoin[b], Yung-Sing Wong[b], Christophe Grangeasse[c], Christine Moriscot[c], Claire Durmort[a], André Zapun[a*] & Cecile Morlot[a*]

[a]Univ. Grenoble Alpes, CNRS, CEA, IBS, F-38000 Grenoble, France

[b]Univ. Grenoble Alpes, CNRS, DPM, UMR5063, 38000 Grenoble, France

[c]Molecular Microbiology and Structural Biochemistry, Université de Lyon, CNRS, UMR5086, 69007 Lyon, France

[1] These authors contributed equally

[*] Correspondence: cecile.morlot@ibs.fr and andre.zapun@ibs.fr

Preprint server: BioRxiv doi: https://doi.org/10.1101/2024.10.18.619035 CC-BY-NC-ND 4.0 International license

Classification: Biological Sciences, Microbiology

Keywords: bacterial cell wall / teichoic acid / click chemistry / super-resolved microscopy / dSTORM / CEMOVIS

Abstract

Teichoic acids (TA) are linear phospho-saccharidic polymers and important constituents of the cell envelope of Gram-positive bacteria, either bound to the peptidoglycan as wall teichoic acids (WTA) or to the membrane as lipoteichoic acids (LTA). The chemical composition of TA varies greatly but the presence of both WTA and LTA is highly conserved, hinting at an underlying fundamental function that is distinct from their numerous specific roles in diverse organisms. We report here the observation of a periplasmic space in the Gram-positive *Streptococcus pneumoniae* by cryo-electron microscopy of vitreous section. The thickness and appearance of this region change upon deletion of genes involved in the attachment of teichoic acids, supporting the role of TA in the maintenance of a periplasmic space in Gram-positive bacteria as their main universal function. Consequences of these mutations were further examined by super-resolved microscopy (dSTORM), following metabolic and fluorophore coupling by click-chemistry in pulse and pulse-chase experiments. This novel labeling method also enabled the titration the actual amount of TA per cell and to determine the ratio of WTA to LTA, to follow the change of TA length during growth phases, and to discover that a mutant devoid of LTA accumulates the membrane-bound TA precursor, that may compensate the absence of LTA. Most importantly, the possibility to follow TA during cell fractionation led to the discovery that LTA containing membranes sediment at low centrifugal forces, allowing easy separation.

Significance

The existence of a periplasmic space in Gram-positive has long been debated. The finding that compromising the attachment of teichoic acids changes the appearance and thickness of the periplasm in the pneumococcus indicates a role of these polymers in the maintenance of this space between the membrane and the cell wall. Using metabolic labeling and electrophoresis showed that LTA-containing membranes are easily sedimented. This finding casts doubts on previous results, since most LTA were likely unknowingly discarded in these studies. Our method of TA analysis opens a new era in the investigation of these important and poorly known bacterial polymers and their role in the periplasmic space of Gram-positive organisms.

Introduction

Teichoic acids (TA) are major components of the cell envelope of Gram-positive bacteria. TA are complex linear polysaccharides attached either to the plasma membrane (lipoteichoic acids, LTA) or to the peptidoglycan (PG) (wall teichoic acids, WTA) (1–3). Although generally non-essential, LTA and WTA participate in numerous cellular processes such as cell wall elongation and hydrolysis, cell division, transport processes, cation homoeostasis, resistance to antimicrobial peptides, and interactions with the environment or the host.

In studies of Gram-positive bacteria (*Bacillus subtilis*, *Staphylococcus aureus*, *Enterococcus gallinarum* and *Streptococcus gordonii*) by cryo-electron microscopy of vitreous sections (CEMOVIS (4)), a region between the cytoplasmic membrane and the cell wall was proposed to be a periplasmic space (5–7). A most interesting speculation is the possible role of TA in maintaining this periplasmic space, so that it would be isotonic with the cytoplasm (**Fig. 1A**) (8).

In most organisms, LTA and WTA have different compositions and are assembled and exported by different pathways (1, 3). TA of streptococci of the *mitis* group, such as *S. pneumoniae*, are particular in two ways: LTA and WTA are products of the same biosynthetic pathway and are therefore of very similar composition, and they are uniquely decorated by phosphocholine residues (**Fig. 1B**) (2).

The role of TA in the pneumococcus is also critical because 13 to 16 different proteins (choline-binding proteins) are anchored to the cell envelope by the interaction of their choline-binding domain to phosphocholine residues (9). The functions of the choline-binding proteins are diverse, several of them are acting on the cell wall itself as hydrolases such as LytA and LytB, others are virulence factors mediating interactions with the host and its immune system.

The pneumococcus has a strict nutritional requirement for choline, which is solely incorporated in its TA (10). However, numerous derivatives can substitute for choline, as long as the hydroxyl group is present and the amine substituents are not too bulky (11). Nutritional shift between choline and ethanolamine had been used in early studies of the localization and composition of nascent cell wall (12). More recently, we have used the incorporation of alkyne- and azido-choline (aCho) derivatives to label TA with clickable-fluorophores and investigate the spatial and temporal relationship between TA and PG assembly by fluorescence microscopy (13, 14).

The pneumococcal repeating unit of TA consists of a pseudo-pentasaccharide ((→4)-6-O-P-Cho-α-D-Gal*p*NAc-(1→3)-6-O-P-Cho-β-D-Gal*p*NAc-(1→1)-Rib-ol-5-P-(O→6)-β-D-Glc*p*-(1→3)-AATGal*p*-(1→)) (SI **Fig. S1**) (15). The glucose (D-Glc*p*) and the ribitol (Rib-ol) are joined by a phosphodiester bond. The two N-acetylgalactosamine (D-Gal*p*NAc) are substituted on position 6 with a phosphocholine, as mentioned above. The phosphocholine is sometimes lacking on the proximal Gal*p*NAc of some subunits, as well as from both Gal*p*NAc from the terminal unit. Subunits are linked together by α-(1→6) bonds. In LTA, the acetamido-4-amino-6-deoxygalactopyranose (AATGal*p*) of

the first subunit is β-(1→6)-linked to the glucose of a mono-glucosyl-diacyl-glycerol (DGlc*p*-DAG) (16). In WTA, the first AATGal*p* is thought to be α-linked via a phosphodiester to position 6 of the PG N-acetyl muramic acid, as in WTA of other species, although this labile linkage has never been experimentally observed in *S. pneumoniae* (15, 17).

Like other surface polysaccharides such as the PG or the capsule, the basic unit is intracellularly synthesized at the plasma membrane onto the carrier lipid undecaprenyl pyrophosphate by a succession of glycosyl- and phosphotransferases (2). The basic unit precursor is then thought to be flipped across the membrane by the flippase TacF (*spr1150*) to allow elongation of the TA polymers at the cell surface by the polymerase TarP (*spr1222*) (18–20). Once on the external surface of the membrane, the polymerized precursors can undergo two fates (**Fig. 1B**). A phosphotransferase can anchor the polymer onto the PG to yield WTA. Alternatively, a glycosyltransferase can transfer the polymer to DGlc*p*-DAG to form LTA. The phosphotransferase attaching WTA is thought to be LytR (*spr1759*) (21), although LytR and the two homologous enzymes Cps2A (*spr 0314*) and Psr (*spr1226*) that form the LCP (LytR-Cps2A-Psr) family may exhibit some redundancy (22, 23). The glycosyltransferase producing LTA was found to be TacL (*spr1702*), since the purification procedure normally yielding LTA produced no detectable TA compounds from a Δ*tacL* strain (24).

Some fundamental aspects of the pneumococcal biology have recently been proposed to rely on shifting the ratio of WTA to LTA. Notably, competence, the process allowing incorporation of DNA from the extracellular environment, was found to be accompanied by an increase of the amount of WTA dependent on the presence of the phosphotransferase LytR (21). In contrast, autolysis, which occurs during the stationary phase of planktonic cultures and is mostly driven by the PG amidase and choline-binding protein LytA, was shown to depend on the amount of WTA, modulated by the phosphodiesterase WhyD that releases TA from the PG (25).

In this work, using CEMOVIS (cryo-electron microscopy of vitreous thin section), we report the existence of a periplasmic space in *S. pneumoniae* WT, Δ*tacL* and Δ*lytR* strains. The observed differences in the appearance and thickness of the periplasmic space supports a participation of TA to its maintenance. The sites of TA incorporation in the cell wall were examined by the metabolic incorporation of aCho and subsequent secondary fluorescent labeling that allowed imaging by super-resolved microscopy, to reveal consequences of the absence of TacL and LytR. In addition, the discovery of the unexpected and previously unreported sedimentation property of the LTA containing-membranes of *S. pneumoniae* allows the simple separation and analysis by gel electrophoresis of labeled LTA and WTA in different strains and conditions. This novel simple method of TA analysis will prompt the reassessment of previous findings, notably regarding the ratio of LTA to WTA in various cellular processes.

Results

Cryo-electron microscopy analysis of *S. pneumoniae* cell envelope

CEMOVIS is a cellular cryo-electron microscopy method that previously provided evidence for a periplasmic space in several Gram-positive bacteria (7, 26). To investigate the contribution of TA to the architecture of the cell envelope of *S. pneumoniae*, we applied the CEMOVIS (SI **Fig. S2**) to the WT (wild-type) strain and two mutants thereof thought to be deficient in the attachment of TA to the cell wall (Δ*lytR*) or to the plasma membrane (Δ*tacL*) (21, 24).

As in other bacterial species, CEMOVIS reveals the existence of a periplasm in WT *S. pneumoniae*, as evidenced by a light region observed between the plasma membrane and the PG (**Fig. 2**). Within this light region, a single dark line runs parallel to the membrane. This observation in *S. pneumoniae* supports the idea that a periplasmic space exists in Gram-positive bacteria, and that this space contains organized material, which was previously described as a granular layer (7).

If a Gram-positive periplasm filled with TA exists, it must contain LTA, which are anchored in the plasma membrane, and possibly WTA protruding from the inner face of the PG layer (8). This hypothesis predicts that variations in LTA and/or WTA incorporation should modify the architecture of the cell envelope. Strikingly, the granular layer present in the WT strain completely disappears in Δ*lytR* and Δ*tacL* cells, (**Fig. 2**). In the absence of TacL, the thickness of the periplasmic space is significantly reduced by (34 ± 5)% (SE) compared to that of the WT strain (**Table 1**), supporting the idea that LTA occupy the periplasmic space. Similarly, the absence of LytR induces a significant reduction of the periplasm thickness ((29 ± 5)% (SE), **Table 1**), suggesting that WTA also participate in the maintenance of this region. The thickness of the periplasmic spaces in Δ*tacL* and Δ*lytR* strains does not differ significantly from each other. In order to increase the signal-to-noise ratio of our cryo-EM images, we took advantage of the exceptional grid adhesion of one vitreous ribbon of Δ*tacL* cells (SI **Fig. S2**) to perform CETOVIS (cryo-electron tomography of vitreous sections). The reconstructed cryo-electron tomogram confirmed the absence of the granular layer throughout the entire volume of a Δ*tacL* cell section (SI **Figs S2A-B**).

Interestingly, CEMOVIS data obtained from the WT, Δ*lytR* and Δ*tacL* strains also showed that the thickness of the PG layer itself is affected when WTA or LTA assembly is impaired (**Fig. 2**, **Table 1**). Indeed, we observed a significant reduction of the cell wall thickness of (17 ± 5)% (SE) or (36 ± 4)% (SE) in the absence of TacL or LytR, respectively. Consistent with the fact that WTA are covalently linked to the PG, the reduction in the cell wall thickness is more pronounced in Δ*lytR* cells compared to Δ*tacL* cells. In contrast to the CEMOVIS method, transmission electron microscopy analysis of sectioned stained freeze-substituted resin-embedded samples (SI **Fig. S3C**) did not reveal measurable differences between the cell wall of the WT and mutant strains. The differing appearance of Gram-

positive cell envelope using the CEMOVIS and freeze-substitution methods, and the difficulty of evidencing the periplasmic space with the latter, was observed an discussed before (26).

Cellular localization of TA insertion

Intrigued by the effect of the absence of TacL or LytR on the ultrastructure of the cell envelope, we examined how the deletion of *tacL* or *lytR* impacts the localization of TA assembly in *S. pneumoniae* cells. To localize newly synthesized TA, an excess of aCho was added for 5 min to exponentially growing cell cultures. Cells were then fixed prior to secondary labeling by strain-promoted azide-alkyne cyclo-addition (SPAAC) click reaction with the DBCO-linked fluorophore Alexa Fluor 647 (DBCO-AF647), following a protocol adapted from (27). As expected, TA insertion occurs at the division site (SI **Fig. S4**). Although the morphology of Δ*tacL* cells is altered, with pointy poles and some expanded and shrunk cells, enriched aCho incorporation was also detected at midcell. In the Δ*lytR* strain, in contrast to the WT parental and Δ*tacL* strains, the 5-min incubation with aCho yielded only a weak midcell labeling in few cells (SI **Fig. S4**). The weak labeling of Δ*lytR* cells may reflect one or a combination of the following: TA are less abundant, cells incorporate less aCho into TA, cells grow more slowly, so that the 5 min pulse represents a shorter fraction of their cell cycle.

The photophysical properties of AF647 are amenable to direct stochastic optical reconstruction microscopy (dSTORM), which allowed the reconstruction of super-resolved images as presented in **Fig. 3**, showing the localization of fluorescent TA after a 5-min labeling pulse experiment. Corresponding images in conventional fluorescence and bright field mode are shown in SI **Fig. S5**. In the three strains, TA were mostly inserted at the division site, where the PG is assembled (28). However, some localizations were also detected elsewhere at the cell surface in all three strains. This heterogenous labeling was similar in all three strains, rendering the weak labeling at the division site of Δ*lytR* cells difficult to identify. This is in contrast to what is observed with PG insertion, where very little signal is observed outside of the cell division zone (**Fig. 3** and Trouve et al. 2021). The localization patterns of newly incorporated TA observed in these experiments are mostly that of WTA, since this distribution is preserved in sacculi preparations (SI **Fig. S5B**). The bright spots that were often seen in sacculi likely correspond to aggregated material that is trapped inside unbroken sacculi.

While there is no discernible difference between the WT and Δ*tacL* cells in the distribution of TA labeled during a 5-min pulse, the evolution of this distribution following a chase, when growth is pursued for up to 35 min (about one WT generation time) without aCho, is markedly different between the two strains (**Fig. 3**). In the WT strain, the separated banded pattern expected from the insertion of unlabeled TA at the division site is observed, mirroring the patterns produced by PG labeling. After 35 min of chase, most WT cells show polar or equatorial labelings following completion of their division. In contrast, in Δ*tacL* cells, labeled TA can be seen over the whole new cell surface that is generated during the pulse and the first 15 min of chase. An unlabeled region is visible at midcell in Δ*tacL* cells

only after 35 min of chase. The chased pattern of labeled PG in the Δ*tacL* strain is not affected and is similar to that in WT.

In dSTORM imaging of the Δ*lytR* strain, the patterns are difficult to discern and many cells show no specific midcell labeling. When visible, the labeled area extends during the chase, as described above for the Δ*tacL* strain.

Separation of labeled LTA and WTA by low-speed centrifugation

In previous studies, unlabeled TA from the pneumococcus have been analyzed by polyacrylamide gel electrophoresis in the presence of SDS (SDS-PAGE). Purified WTA were revealed in gel by an Alcian blue staining procedure, whereas LTA from crude membrane fractions were revealed by immune-blotting with anti-phosphocholine antibodies (e. g. (Flores-Kim et al. 2019; 2022)). The standard preparative purification of TA from *S. pneumoniae* starts with the sedimentation of mechanically broken cell walls, which contain the WTA, with the concomitant detergent solubilization of LTA (e.g. (24)). Alternatively, for analysis of LTA by immuno-blotting for example, protoplasts prepared by PG enzymatic digestion would be osmotically lysed, cellular debris would be sedimented by low-speed centrifugation and discarded, and LTA-containing membranes would finally be collected by ultracentrifugation (e. g. (25, 29)). On the other hand, WTA can be released from cell wall fragments by thorough digestion of the PG (e. g. (17, 24)) or alkaline hydrolysis (e. g. (25, 29)).

Since we were able to fluorescently label TA, we thought it would allow simpler in-gel analysis. WT cells were cultured over two generations in C-medium devoid of choline but supplemented with 200 µM aCho. Cells having thus metabolically incorporated aCho were lyzed by overnight digestion of the cell wall with lysozyme, mutanolysine and recombinant LytA. The aCho was coupled to a DBCO-fluorescent Alexa dye (AF488) by strain-promoted azide-alkyne click reaction during the lysis incubation. The lysates were then cleared of debris by a low-speed centrifugation at 10,000 *g*, and ultracentrifugation of the supernatant at 100,000 *g* was subsequently performed to separate the membrane from the soluble fraction. Since at this stage the TA were fluorescently labelled, we were surprised to find more fluorescence in the low-speed pellet than in the pellet resulting from the ultracentrifugation. Analysis of the soluble fraction (the supernatant) by SDS-PAGE showed the pattern expected from labeled WTA migrating as a set of poorly resolved bands with low electrophoretic mobility, as in typical Alcian blue-stained gels (**Fig. 4A**). The pattern expected from labeled LTA, a ladder of well-resolved bands with a greater electrophoretic mobility than the WTA, was observed chiefly in the low-speed pellet. Centrifugation of cells lysates with labeled TA at different speeds confirmed that 2 min at 20,000 *g* were sufficient to sediment most of the LTA (**Fig. 4A**). The nature of high-mobility species and other details on the fractionation and the electrophoresis are commented in the SI (Notes on the fraction of LTA and WTA, SI **Fig. S6**; Notes on the electrophoresis, SI **Fig. S7**).

Coomassie blue staining of electrophoresis gels of the supernatant and pellets of low-speed centrifugation showed that the pellet and supernatant have different protein profiles (SI **Fig. S8A**). After chloroform extraction, iodine-stained thin layer chromatography showed that the low-speed pellet contained most of the lipids (SI **Fig. S9A**) and negative-stain transmission electron micrograph of the low-speed pellet revealed membranous material (SI **Fig. S9B**). Taken together, these observations indicate that the LTA-containing membrane fraction of lysed *S. pneumoniae* cells sediments when submitted to low relative centrifugal force.

NMR analysis of LTA prepared after low-speed centrifugation

To determine that the low-speed sedimentation of LTA-containing membranes was not an artifact of the labeling method, we applied the same separation method to unlabeled cells followed by the the extraction procedure previously reported (24) for NMR analysis. The ^{31}P NMR spectrum showed the presence of the typical TA phosphorus peaks from internal and terminal units (SI **Fig. S10**). Subsequent treatment with hydrazine to remove acyl chains improved the spectra as expected (16). Natural abundance ^{13}C,^{1}H-HSQC spectrum showed the presence of the expected sugar species, including the glucosyl-glycerol from the lipid anchor of LTA (A and GRO peaks, SI **Fig. S10**).

Titration of cellular TA

The fluorescent labeling of TA by click chemistry and separation of LTA and WTA allowed the titration of the different species in cells. For this, we incubated varying quantities of the aCho-labeled cell lysate with fixed amounts of DBCO-AF488. Samples were analyzed by gel electrophoresis and the relative amount of the various fluorescent species was determined by densitometry and plotted against the concentration of cells. The gels and quantifications are shown in **Figs 4B-C** and SI **Figs S11A-B** for two concentrations of DBCO-AF488. For intermediate amounts of lysate, the concentrations of clickable groups were too low to reach reaction completion during the incubation time. Only with the highest amount of lysate could the fluorophore be nearly consumed. However, for low amounts of lysate, when the fluorophore is in large excess, the reaction is also expected to have neared completion. Therefore, the fraction of unreacted DBCO-AF488 was linearly extrapolated to zero from the measurements at low lysate concentrations, to obtain the amount of lysate that would titrate the fluorophore in an infinite reaction time. Thus, 1.9 µM DBCO-AF488 would titrate the metabolized aCho from (0.24 ± 0.01) × $2.8{\cdot}10^{8}$ cells·mL^{-1} and 3.7 µM would titrate aCho from (0.45 ± 0.01) × $2.8{\cdot}10^{8}$ cells·mL^{-1} (**Figs 4B-C** and SI **Figs S11A-B**), which is equivalent to $(17 \pm 2){\cdot}10^{6}$ incorporated aCho molecules per cell. Since about 55% of labeled choline are incorporated into TA, the rest being found in the form of phosphocholine, there are about $(9.4 \pm 1.1){\cdot}10^{6}$ labeled TA choline per cell. Over two generations grown in the exclusive presence of labeled choline, at most 75% of TA choline residues are expected to be labeled, as measured previously (13). The total amount of TA choline residues per

cell can therefore be estimated to be about $(12.5 \pm 1.5)\cdot10^6$. As the major species of TA consists of 6 repeating units (16, 17), with each unit comprising about two choline residues, the number of TA molecules per cell is about 10^6.

Although the electrophoretic mobility of the longest species of LTA overlaps that of the shortest WTA species, the major species are well separated (**Figs 4B-C** and SI **Figs S11A-B**) and allowed their relative quantification. Labeled choline residues incorporated into LTAs were found to account for 15 ± 5 % of the TA choline residues. Assuming a similar size distribution of LTA and WTA, LTA and WTA represent roughly 15 and 85% of pneumococcal TA, respectively.

Evolution of TA along *S. pneumoniae* growth phases

Using TA labeling and sedimentation separation, we examined whether changes in the distribution of TA could be detected during growth. WT and Δ*lytA* cells were grown with aCho over two generations. LytA is the main autolysin of *S. pneumoniae*, and culture of cells lacking this PG hydrolase show an extended stationary phase with minimal lysis. Cells were harvest during the exponential phase of growth, at the onset of the stationary phase, and when the WT cells started to lyse. Remarkably, longer species of LTA can be observed at later stages of growth (**Figs 5A-B** and SI **Fig. S12A**). Assuming that the most abundant form consists of 6 repeating units, the 5- and 7-unit species are the next most abundant species, and traces of the 8- and 9-unit species can be detected during the exponential phase of growth. Later during the culture, although the 6-unit species remains the most abundant and the 5-unit is detected at level comparable as earlier in the culture, longer species become more abundant with up to 17 identifiable units. Surprisingly, the size distribution appears to be bimodal with a first group of species consisting of 5 to 11 units, and a second group of longer forms where the most abundant one contains 15 units. When considering the electrophoretic pattern, it should be considered that the signal of the different species is proportional not only to their amount, but also to their length, since longer species harbor more labeled choline residue. Therefore, long species are less abundant than they appear.

There was no significant difference between the strains with and without LytA (**Figs 5A-B** and SI **Fig. S12A**). The Δ*lytA* did not lyse spontaneously, but a similar amount of TA with the same distribution was obtained from the lysing *lytA*$^+$ culture. Thus, although the WT cells lyse, their WTA and LTA are not degraded and remain unchanged in the medium.

We also monitored the fate of the labeled species during a chase period of further growth following a 5-min labeling pulse of WT cells, mirroring the dSTORM observations. No modification of the pulse-labeled TA could be detected during the chase time, whether the growth, labeling pulse and chase were performed in BHI or C-medium and supplemented with yeast extract (**Fig. 5C** and SI **Fig. S12B**).

297

298 **LTA and the role of TacL**

299 WTA and LTA were examined in a strain devoid of TacL, which is thought to be responsible for
300 the attachment of LTA to membrane glycolipids (**Fig. 6A**). Labeled TA were found in the pellet, and
301 when analyzed by gel electrophoresis were indistinguishable from LTA. After double checking that the
302 strain was indeed deleted for the *tacL* gene, we hypothesized that the sedimented TA could be
303 membrane-bound precursors still attached to the undecaprenyl-pyrophosphate lipid carrier. In support
304 of this idea, pulse-labeled LTA-like bands disappeared during a chase (**Fig. 6B**), as would be expected
305 if these compounds were precursors being transformed into WTA.

306 The pyrophosphate linkage in the PG precursor lipid II is labile at low pH and high temperature
307 (30). Reasoning that the same should be true for the TA precursor, we incubated the sedimented fraction
308 from the WT and Δ*tacL* strain at 110°C at either pH 8 or pH 4.2. The TA sedimented from the Δ*tacL*
309 lysate were degraded at both pH, whereas those from the parental strain were still detected (**Fig. 6C**).
310 This observation suggested that the previously reported failure to isolate TA from the membrane
311 fraction of a Δ*tacL* strain could be due to the process that involves boiling at pH 4.7 (24). To test this
312 hypothesis, we submitted resuspended pellets of labeled TA from the WT and Δ*tacL* strains to the initial
313 steps of the reported isolation procedure for LTA: boiling in SDS at pH 4.7, lyophilization and ethanol
314 wash of the lyophilizate followed by butanol extraction and retention of the aqueous fraction (24).
315 Although material was lost at each step, LTA from WT cells survived the procedure unscathed, whereas
316 pelleted TA from the Δ*tacL* strain was lost at the first step, which involves boiling at low pH (**Fig. 6D**).
317 In that case, labeled material with a lower electrophoretic mobility appeared as a smear like that of
318 solubilized WTA.

319 To confirm that TA sedimented from a lysate of cells devoid of TacL are membrane bound
320 through a pyrophosphate, we incubated these TA with recombinant colicin M from *Pseudomonas*
321 *aeruginosa*. Colicin M are toxins that kill bacteria by hydrolyzing the ester bond between the
322 undecaprenol and the pyrophosphate of the PG precursors lipid I and II (31). Colicin M from *P.*
323 *aeruginosa* was shown to be the most active *in vitro* and to display some activity on undecaprenyl-
324 pyrophosphate without saccharide, thus being less stringent regarding its substrates than other colicin
325 M (32). *P. aeruginosa* colicin M could indeed hydrolyze labeled sedimented TA from Δ*tacL* cells,
326 whereas it was inactive on labeled LTA from WT cells (**Fig. 6E**). The colicin M hydrolytic activity was
327 inhibited by chelation of divalent cation by EDTA, as expected (32).

328 The combined results show that TacL is indeed the glycosyltransferase responsible for the
329 attachment of TA to the membrane glycolipids. However, in the absence of TacL, membrane-bound
330 TA remain present in abundance in the form of undecaprenyl-pyrophosphate-attached precursors.

To evaluate if the membrane-bound TA precursors accumulating in the Δ*tacL* strain are on the inside or outside of the plasma membrane, cells were grown in C-medium in the presence of 0.2 µM aCho, and the secondary labeling with DBCO-AF488 was performed by a 2 h incubation at room temperature either before, or after cell lysis. Samples were analyzed by gel electrophoresis (**Fig. 6F**). LTA in the WT strain or membrane-bound precursors in the Δ*tacL* strain were equally labeled before and after lysis, like WTA. In contrast, cytoplasmic azido-phosphocholine was only labeled after lysis, demonstrating that the DBCO-AF488 probe is membrane impermeant.

LytR is the main WTA phosphotransferase

WTA and LTA were also observed in strain Δ*lytR* which is devoid of one of the three phosphotransferases involved in the attachment of surface polysaccharides (the LCP enzymes), although WTA are less abundant and LTA appear to be longer (**Fig. 6A**). In the WT strain, labeled choline in WTA in this particular experiment was found to represent ~ 80% of the total labeled cholines in TA, whereas in the Δ*lytR* strain, this proportion was decreased to ~ 51%. Relative to LTA, the amount of WTA is decreased about four-fold in the absence of LytR.

In C-medium, the Δ*lytR* strain grew more slowly and reached a lower cell density than its parental strain (SI **Fig. S13**). While the WT cells were harvested during their exponential phase of growth, this could not be achieved with Δ*lytR* cells that were collected at the end of their growth phase to obtain sufficient material for analysis. The longer LTA observed in the Δ*lytR* strain may therefore result from the cells entering the stationary phase (like the WT strain in **Fig. 5A**), rather than from the absence of LytR.

Discussion

Multiple roles have been found for TA in various bacteria. These varied functions, however, fail to explain why the presence LTA and WTA with different compositions is conserved in Gram-positive organisms. An underlying common function based on the attributes shared by TA in different species must lie at the root of the conservation of these cell wall polymers through evolution. The hypothesis proposed by Erickson posits that TA are necessary to maintain a periplasmic space at an osmotic pressure that counter balances that of the cytoplasm (8). TA being maintained for this reason may then have been coopted by evolutionary process to carry out additional functions, like evolutionary spandrels (33). This attractive hypothesis is however difficult to test, not least because data supporting the existence of a periplasmic space in Gram-positive bacteria are scarce.

Here, our CEMOVIS images of *S. pneumoniae* (**Figs 1** and SI **S3A-B**) reveal the presence of a region of lower electron density between the membrane and the PG, as reported previously with other Gram-positive organisms and defined as periplasmic space (5–7). About halfway between the PG and the membrane, this periplasmic space appears to be partitioned by a thin layer of more electron dense material, termed the granular layer in a previous study of *S. gordonii* (7). By contrast, freeze-substitution and osmium staining produced thin section of cells with no visible periplasm (SI **Fig. S2C**). Since high-pressure frozen cells are directly sectioned for CEMOVIS but undergo numerous subsequent treatments for freeze-substitution and contrasting, it is tempting to consider that the CEMOVIS images yield more truthful representations of the cellular architecture. The thinning of the periplasmic space and disappearance of the granular layer in strains with diminished amounts of either WTA (Δ*lytR*) or LTA (Δ*tacL*) support Erickson's hypothesis that a periplasmic space is maintained by the physical properties of WTA emanating from the PG layer and LTA springing from the membrane (8). In this framework, it is also striking that the appearance of the cell envelope of *S. gordonii* (7) and *S. pneumoniae* are so similar, despite the fact that the composition of their TA are very different (2, 34, 35), lending credence to a fundamental function of TA stemming from their general physico-chemical properties, rather than from specific molecular interactions.

Erickson listed four physical mechanisms of the polyelectrolyte brush model of TA that could explain the formation of a periplasmic space where TA chains closely packed on a surface of the plasma membrane generate a pressure when pushed against another TA covered surface (the PG layer). These four contributing factors are: "(1) excluded volume, where the chains cannot occupy the same space; (2) electrostatic repulsion within and between chains; (3) reduced entropy of the chains as they are confined to a narrow cylinder; (4) reduced entropy of the counterions as they are concentrated near the anionic charges" (8). Although generally applicable, the electrostatic repulsion experienced by most anionic TA cannot apply to TA from *S. pneumoniae*, since these are zwitterionic and polyampholytes. Indeed, the phosphocholine side chains carry both a positive and a negative charge at physiologically relevant pH (zwitterionic), while the main chain repeated unit also carry one negative chain from its

phosphodiester linkage and one positive charge from the amino-group of its AATGal*p* ring (polyampholyte character). Being globally neutral, pneumococcal TA may not attract counterions, which therefore would not contribute to the osmolality and pressure of the periplasmic compartment. Consequently, the excluded volume and reduced entropy of TA due to confinement, of the neutral brush polymer theory (36), could be the main drivers of the maintenance of a periplasmic space in streptococci of the *mitis* group. Since *S. pneumoniae* and *S. gordonii* display similar periplasmic spaces when observed by CEMOVIS, despite having TA with different electrostatic properties, future comparisons of these species in different pH, osmolality and ionic strength regimen may provide clues about the physico-chemical interactions of these polymers.

The brush polymer model of TA function in forming a periplasmic space applies only if they are present at a density at which volume exclusion occurs. Our metabolic labeling method using aCho that can be titrated with a clickable fluorescent probe has allowed to evaluate the amount of TA chains per cell to about 10^6. Since WTA may be distributed throughout and on both sides of the PG layer, let us concentrate on the LTA which are less abundant but are all expected to be in the periplasmic space with about $1.5 \cdot 10^5$ chains per cell. A single pneumococcal cell could be approximated by a sphere with a diameter of 1 µm and surface area of $3 \cdot 10^{-12}$ m^2. Pneumococcus exists mostly as diplococci, so let us assume an average surface area per cell of $5 \cdot 10^{-12}$ m^2. The surface density of LTA would therefore be $3.3 \cdot 10^{16}$ molecule$\cdot m^{-2}$ or one LTA chain per 30 nm^2. This density value is lower than that of one chain per 5 nm^2 calculated for LTA from *Staphylococcus aureus* based on the ratio of LTA to membrane lipids (8). Although both density values are rough estimates, they require volume exclusion to accommodate TA chains at the membrane surface and are therefore compatible with the polymer brush model.

The morphogenesis and cell division of Gram-positive bacteria rely on the carefully orchestrated assembly of the cell envelope, which includes the membrane, the PG layer and the TA. To gain a better understanding of the incorporation of TA in the cell wall, TA were metabolically labeled with aCho that allowed the subsequent grafting of fluorescent probes. Cells labeled during short pulses of incubation could be observed by dSTORM, revealing the regions of TA insertion in unprecedented details. In parallel, labeled TA, after short pulses or continuous growth in labeling media, could be analyzed by gel electrophoresis after cell wall digestion by PG hydrolases. As expected from an earlier study with conventional microscopy (Bonnet et al. 2018), TA are incorporated in the cell wall at the division site (**Fig. 3** and SI **Figs S4** and **S5**). Patterns after a 5-min labeling pulse are very similar to those obtained when the PG is pulse-labeled (28) and do not differ in the absence of the glycosyltransferase TacL. In contrast, the absence of the phosphotransferase LytR markedly reduce the fluorescence signal. These observations are consistent with the role attributed to TacL of anchoring the less abundant LTA, and to LytR of attaching the more abundant WTA. The electrophoretic analysis of labeled TA confirmed that WTA are less abundant in the Δ*lytR* strain (**Fig. 6**). The amount of LTA

appeared comparable in WT and Δ*lytR* cells, but LTA seem to contribute little to the dSTORM localization patterns, since cell wall sacculi that lacks LTA show patterns identical to that of whole cells (SI **Fig. S5B**).

The notable difference with TA compared to PG is the presence of some heterogenous surface localization after a labeling pulse. This surface signal is not due to non-specific binding of the fluorophore to the surface, since it is not observed in labeling studies of the PG (28). Since the same level of heterogenous surface labeling was observed with the three strains investigated, the most likely reason is some non-specific adsorption of aCho at the cell surface. It is also possible that some LTA or membrane-bound precursors, which are not covalently bound to the cell wall, can diffuse from the division site across the plasma membrane during the pulse and prior the fixation. Finally, it is possible that hitherto unidentified choline-containing compounds at the cell surface are also labeled.

When imaging was performed after a chase time during which cells are allowed to grow in the absence of probes following the labeling pulse, patterns of labeled TA in Δ*tacL* and Δ*lytR* cells appeared different from those produced when the PG was labeled (**Fig. 3**). In WT cells, in contrast, TA and PG labeling patterns were similar throughout the chase time. Although the appearance of pulse labeled Δ*tacL* cells resemble that of WT cells, the labeling patterns are strikingly different after a chase period. In Δ*tacL* cells, all the cell wall generated during the chase is labeled, resulting in a wide contiguous fluorescent region, whereas it is not labeled in WT cells, producing separated bands. It is most likely that in WT cells, production of WTA and LTA are competing pathways as the two polymers share the same composition, that rapidly consumes the undecaprenyl-linked polymerized TA precursors, whereas these precursors accumulate in the Δ*tacL* strain (**Figs 6B-E**). The slower turnover of the undecaprenyl-linked TA in the Δ*tacL* strain allows the cell wall incorporation of labeled WTA during the chase, several minutes after the aCho has been removed from the medium. This phenomenon could be observed in an electrophoretic analysis of a pulse-chase labeling experiment of the Δ*tacL* strain, where membrane bound TA precursors disappear over a 15-min course (**Fig. 6B**). Patterns are difficult to discern in the Δ*lytR* strain due to the weak labeling signal, however, they appear to resemble those of Δ*tacL* cells.

In streptococci of the *mitis* group, TA serve as moorings for the attachment of a variety of surface proteins termed choline-binding proteins, because the interaction occurs between the choline residues of TA and protein domains made of repeated choline-binding motifs. The functions of these proteins are varied, playing roles in virulence, competence, or cell wall metabolism (9). The localization of some choline-binding protein can be highly restricted, such as that of the autolysin LytA, which is found at mid-cell to hydrolyze the PG to promote lysis, or the other cell wall hydrolase LytB that localizes to the new poles to complete cell separation (37, 38). Since the choline-binding domains of these proteins participate in their localization (37, 39), it probably requires that TA at different places of the cell surface display some compositional or size differences, that could arise from some maturation process.

To investigate this possibility, we analyzed metabolically labeled TA at different stages of cell culture (**Figs 5A-B** and SI **S12A**). Interestingly, longer LTA are present when the culture enters its stationary phase. One can speculate that the same may be true with WTA, although this could not be determined in our experiment. Surprisingly, when pulse labeling is performed at the onset of stationary phase, the LTA that are synthesized during that phase of the culture do not differ from those produced earlier during the exponential phase, despite the observation of longer LTA are present in late phase culture (**Figs 5A-B** and SI **S12A**). How could these long LTA arise? Since their length distribution is bi-modal and the longer (12-16 units) are about twice the size of the short ones (5-7 units), it is tempting to imagine that they may arise from the coupling of pre-existing TA.

The finding that undecaprenyl-attached TA accumulate in the Δ*tacL* strain to a level that is lower, but comparable to that of LTA in a WT strain raises the question of whether these precursors can fulfill the function of mature LTA, at least partially. The observation by CEMOVIS that the cell envelope architecture is altered in Δ*tacL* cells, with a thinner periplasmic space devoid of granular layer (**Fig. 1**), indicates that if some functional replacement occurs, it is not complete. It has been proposed previously that the physical properties of the undecaprenyl chain underlie the localization of the PG precursor lipid II at the sites of cell wall assembly, which occurs at sites of maximal membrane curvature (40). The same reasoning would restrict the presence, and thus the function, of the undecaprenyl-linked TA precursors to sites of cell wall assembly were they can be incorporated into WTA or true LTA. In the absence of TacL, undecaprenyl-linked TA accumulate to a greater extent, so that their turn over is slower than in a WT strain, resulting in the incorporation of labeled WTA during a chase after the labeling pulse (**Fig. 3**).

The propensity of *S. pneumoniae* membrane to sediment at low centrifugal speed, discussed in the SI, is not without experimental consequences in the study of TA. A number of recent studies have sought to investigate the possible role of changes in the relative proportion of WTA and LTA in physiological processes such as the autolysis or the competence (21, 25, 29). However, it is likely that most of the LTA-containing membranes were unknowingly discarded in these experiments during a clarification step of cell lysates, casting doubts on the reported ratio of WTA to LTA and the associated conclusions. The metabolic labeling and electrophoretic analysis methods reported here will certainly help to reappraise several aspects of the biology of TA in *S. pneumoniae*.

Acknowledgements and funding sources

We thank D. Fenel from the IBS for performing the negative stain TEM, and T. Touzé from the Université Paris Saclay for the generous gift of purified colicin M. We thank O. Glushonkov, J.-P. Kleman for advice and support regarding dSTORM; G. Schoehn for electron microscopy. We thank H. Erickson from Duke University for sharing thoughts about TA and periplasmic space.

Support for this work comes from the Agence Nationale de la Recherche (ANR-23-CE11-0029 to CeM, ANR-19-CE15-0011 to CG, and ANR-19-CE07-0035 to YSW). EB received funding from GRAL, a program from the Chemistry Biology Health (CBH) Graduate School of University Grenoble Alpes (ANR-17-EURE-0003), and from the Ecole Doctorale Chimie et Sciences du Vivant of the University Grenoble Alpes. IBS acknowledges integration into the Interdisciplinary Research Institute of Grenoble (IRIG, CEA). This work used the platforms of the Grenoble Instruct-ERIC center (ISBG ; UAR 3518 CNRS-CEA-UGA-EMBL) within the Grenoble Partnership for Structural Biology (PSB), supported by FRISBI (ANR-10-INBS-0005-02) and Labex GRAL and ARCANE, financed within the University Grenoble Alpes graduate school (Ecoles Universitaires de Recherche) CBH-EUR-GS (ANR-17-EURE-0003). The IBS/ISBG electron microscope facility is supported by the Auvergne-Rhône-Alpes Region, the Fondation Recherche Médicale (FRM), the fonds FEDER and the GIS-Infrastructures en Biologie Santé et Agronomie (IBISA).

Authors contributions

Mai Nguyen : Formal Analysis ; Investigation ; Visualization ; Writing – review and editing. **Elda Bauda** : Formal Analysis ; Investigation ; Visualization ; Writing – review and editing. **Cédric Laguri** : Formal Analysis ; Investigation ; Writing – review and editing. **Célia Boyat** : Investigation. **Céline Freton** : Investigation ; Resources. **Anne Chouquet** : Investigation. **Benoit Gallet** : Investigation. **Morgane Baudoin** : Investigation; Resources. **Yung-Sing Wong** : Funding acquisition; Resources ; Supervision ; Writing – review and editing. **Christophe Grangeasse**: Resources ; Supervision ; Writing – review and editing. **Christine Moriscot** : Supervision ; Writing – review and editing. **Claire Durmort** : Funding acquisition ; Methodology ; Writing – review and editing. **André Zapun** : Conceptualization ; Investigation ; Methodology ; Supervision ; Visualization; Writing - original draft ; Writing – review and editing. **Cécile Morlot** : Conceptualization ; Funding acquisition ; Supervision ; Writing – review and editing.

MN and EB contributed equally to this work. MN performed optical microscopy. EB, BG and ChM carried out electron microscopy. MN, CB, AC and AZ carried out biochemical experiments. CL performed NMR experiments. CF and CG designed and produced mutant strains. CD and AZ developed

525 labeling and analysis methods; MB and YSW synthesized aCho. CM and AZ jointly supervised this
526 work.

527

528 ## Competing interests

529 The authors declare no competing interests.

530

531

Materials and methods

Bacterial strains and culture conditions

S. pneumoniae strains are listed in **Table 2**. Glycerol stocks of WT, *ΔlytA, ΔtacL* and *ΔlytR* cells were used to inoculate Bacto™ BHI broth (BD), C-medium (27). Cultures were grown at 37 °C in a static incubator with a 5% CO_2 atmosphere. Two successive dilutions of the cultures were performed to ensure that steady-state growth was reached. To characterize growth phases, cells were grown in 2.5 mL of BHI or C-medium in 24-well plates sealed with a transparent film. Cultures were inoculated at an OD_{600} of 0.03 (or 0.12 for the *ΔlytR* strain in C-medium). In a BMG Fluostar Omega plate reader at 37°C, turbidity was measured at 595 nm every 20 min after 5 s agitation.

High-pressure freezing

Cells at an OD_{600} of 0.2-0.3 were collected by centrifugation. Pellets were supplemented with or without 20% dextran in phosphate-buffered saline (PBS). Pellets supplemented with dextran were drawn into copper tubes. Pellets without dextran were dispensed in 3-mm type A gold/copper platelets, covered with the flat side of a 3-mm type-B aluminum platelet (Leica Microsystems). The samples were vitrified by high-pressure freezing using an HPM100 system (Leica Microsystems) in which cells were subjected to a pressure of 210 MPa at -196°C.

CEMOVIS and CETOVIS

Copper tubes were trimmed at <-140°C in an EM UC7 Cryo-ultramicrotome equipped with a micromanipulator (Leica Microsystems). Ultrathin sections were produced with a 35° diamond cryo-knife (Diatome) at a nominal thickness of 70 nm and at a nominal cutting feed of 50 $mm \cdot s^{-1}$. Sections were transferred onto Quantifoil carbon-covered 200-mesh copper grids using the micromanipulator and an antistatic device for favoring the attachment of the ribbon to the grid. Grids were transferred to a Gatan cryoholder kept at -170°C and inserted into a TF20 cryo-electron microscope (FEI) equipped with a tungsten field emission gun. The accelerating voltage was 200 kV. Specimens were irradiated with a low electron dose. Images were recorded with a CMOS CETA camera at a nominal magnification ranging from x5,000 to x29,000 (pixel size 8.1 to 3.7 Å). No peculiar image processing was performed on the micrograph. For CETOVIS, tilt series were acquired from -50° to + 50° with an increment of 2.5° according to the dose symmetric Hagen scheme. Images were acquired at a defocus of -10 µm at nominal magnification x29,000 (pixel size 3.7 Å). Tilt series were aligned, and tomogram reconstructed using the IMOD software package (41), using the patch tracking method, followed by weighted back projection and SIRT like filter for purposes of representation.

Freeze substitution and ultramicrotomy at room temperature

The freeze substitution and ultramicrotomy protocols were derived from (Bauda et al., 2023). Briefly, following high pressure freezing, the vitrified pellets were freeze-substituted at -90°C for 80 h in acetone supplemented with 2 % OsO_4 (AFS2; Leica Microsystems). The samples temperature was

increased slowly to -60°C (2°C·h^{-1}). The temperature was further raised to -30°C (2°C·h^{-1}) after 8 to 12 h, and finally to 0°C within 1 h. The temperature was decreased to -30°C within 30 min, and rinsed in pure acetone 4 times. The samples were infiltrated with progressively higher concentrations of resin (Embed812, EMS) in acetone, while the temperature was gradually increased to 20°C. Pure resin was supplemented at room temperature. Following polymerization at 60°C for 48 h, 70-nm thick sections were produced using a Leica UC7 ultramicrotome and placed onto formvar carbon-coated 200-mesh copper grids (Agar Scientific). Uranyl acetate (2% during 5 min) was used to stain the sections, followed by a 5 min incubation in lead citrate. After rinsing in water, the sections were imaged using a Tecnai G2 spirit BioTwin (FEI) microscope operating at 120 kV, at nominal magnifications of 11,000 to x23,000 (pixel size of 5.6 to 2.8 Å), with an Orius SC1000B CCD camera (Gatan).

Conventional and super-resolved fluorescence microscopy

Cultures in exponential phase (25 mL, OD_{600} of 0.3) were centrifuged at 3220 *g* at room temperature for 15 min. The bacterial pellets were resuspended in 1/25th original volume of pre-warmed BHI supplemented with either 2 mM azido-D-Ala-D-Ala for PG labeling or 1.5 mM aCho for labeling of the TA, and incubated for 5 min at 37°C water bath (the "pulse" period).

Cells were then pelleted (10,000 *g*, 1 min) and washed with 1 mL BHI before being resuspended in 20 mL of pre-warmed BHI without probe. Immediately, 2 mL of this resuspension were pelleted (10,000 *g*, 1 min) to prepare "pulse-only" samples. The rest of the bacterial culture was allowed to continue growing at 37°C ("chase" period). At 5 min, 15 min and 35 min into the "chase" period, 2 mL were pelleted as described earlier. The pellets were resuspended in PBS containing 2% paraformaldehyde for overnight fixation at 4°C.

For the preparation of sacculi, the "pulse" period was conducted as above. After cells were washed and resuspended in fresh medium, they were allowed to grow further for 15 min. The chased bacterial cultures (19 mL) were centrifuged (3220 *g*, 5 min) and the pellets were washed with 1 mL of 10% sodium dodecyl sulfate (SDS) (10,000 *g*, 1 min). Cells were then resuspended in 1 mL of 10% SDS and incubated at 100°C for 1 h, vortexed every 15 min. Sacculi were washed twice with 500 µL of 80 mM Tris-HCl pH 7 and incubated in 500 µL of a solution containing 20 µg·mL^{-1} DNAse and 20 µg·mL^{-1} RNAse, 20 mM $MgCl_2$ and 80 mM Tris-HCl pH 7 at 37°C with agitation for 1 h, prior to addition of Proteinase K (final concentration 200 µg·mL^{-1}), 2 mM $CaCl_2$, 80 mM Tris-HCl pH 7, and further incubation overnight. Finally, sacculi were washed once with 200 µL of water.

For coupling of fluorophores, cells or sacculi were pelleted (10,000 *g*, 1 min) and resuspended into 50 µL (for fixed cells) or 150 µL (for sacculi) of PBS containing 30 µM DBCO-AF647 (JenaBiosciences). After 45 min at room temperature, samples were washed 3 times with 300 µL PBS. For dSTORM imaging, fluorophore-labeled cells or sacculi were resuspended in a solution containing 100 mM β-mercaptoelthylamine and an oxygen-depleting system consisting of a GLOX enzyme mix

(40 µg·mL^{-1} catalase, 0.5 mg·mL^{-1} glucose oxidase) in 75 mM Tris-HCl pH 8, 25 mM NaCl, and 10% glucose.

Samples were mounted between a microscopy slide and a high-precision coverslip pre-treated with UV light for 20 min. To coax the cells or sacculi into lying on the slide along their longitudinal axis, a heavy weight was applied on top of the cover slip as described previously (27). The edges of the cover slip were sealed with colorless nail polish.

Observations were made with an Abbelight SAFe 360 commercial STORM microscope. For fluorescence signal acquisition, the field was first excited with a 640-nm scanning laser at low power (1%) to capture a low-resolution conventional fluorescence image of the AF647 signal. The laser intensity was then steadily raised to 100%. ASTER technology, implemented in the microscope, provides for a homogeneous sample excitation. In our experiments, the gaussian beam at the power density of 10 kW·cm^{-2} (average, FWHM 50 µm, power 200 mW, measured at the sample) scans the region of interest of 160^2 µm² resulting in 800 W·cm^{-2} of average effective power density. AF647 dye molecules went through cycles of fluorescent state and dark state. When most AF647 fluorophores had displayed this transition (estimated visually by the frequency and density of fluorescence blinking, a set of 15,000 consecutive frames were taken with 50-ms exposure time. A bright-field image of the field was captured afterwards.

The 15,000-frame sets were processed with the FIJI plugin ThunderSTORM, which localizes the center of a Gaussian function fitted to each individual fluorescence signal and returns a data table containing the localization coordinates of all labeled molecules. Correction of drifts occurring during each set of acquisition and reconstruction of the final super-resolution images were performed in the same software.

TA labeling, cell lysis and fractionation for electrophoretic analysis

TA were labeled by growing cells WT or mutant strains in C-medium in the presence of 200 µM aCho to an OD_{600} of 0.5. Cells were harvested, washed and resuspended to an OD_{600} of 15 in 50 mM Tris-HCl pH 8, 150 mM NaCl, 1 mM $MgCl_2$ containing 0.36 mg·mL^{-1} lysozyme, 0.32 mg·mL^{-1} mutanolysine, 0.36 mg·mL^{-1} RNase, 0.36 mg·mL^{-1} DNase, and 25 µM DBCO-AF488. After lysis overnight on wheel at room temperature cells were centrifuged for 2 min at 1,250, 5,000 or 20,000 *g*. The pellets were resuspended in the same volume. An aliquot of the 20,000 *g* supernatant was incubated at 37°C for 2 h with 10 kU of calf intestinal alkaline phosphatase.

Samples were then analyzed by electrophoresis on polyacrylamide gel (12%, acrylamide:bis-acrylamide 29:1) in the presence of 1% SDS with a Tris/tricine buffer system. The gels were imaged by trans-illumination with UV light without saturation on a BioRad Chemidoc imager.

Lipid analysis

R800 cells were grown to an OD_{600} of 0.5 in BHI and harvested by centrifugation for 15 min at 3220 *g*. Cells were washed twice with 1 mL 50 mM Tris-HCl pH 8, 150 mM NaCl, 1 mM $MgCl_2$ and

resuspended in 1 mL of the same solution containing 0.36 mg·mL^{-1} lysozyme, 0.32 mg·mL^{-1} mutanolysine, 0.36 mg·mL^{-1} RNase and 0.36 mg·mL^{-1} DNase. After overnight incubation at room temperature. Half of the sample was centrifuged for 2 min at 20,000 *g*, and the pellet was resuspended in the initial volume of the same buffer. The pellet, supernatant and whole 500 µL fractions were each extracted twice with 500 µL $CHCl_3$. The organic fractions were dried and redissolved in 40 µL $CHCl_3$/methanol (80:20) prior to analysis by thin layer chromatography on 0.2 mm silica plates (Macherey-Nagel Xtra SIL G) developed with $CHCl_3$/methanol/acetic acid (80:15:8) and stained with iodine vapour.

Negative stain electron microscopy of pellets

Negative Stain-Mica-carbon Flotation Technique (MFT)-Valentine procedure was applied (42). Samples were absorbed to the clean side of a carbon film on mica, stained and transferred to a 400-mesh copper grid. The images were taken under low dose conditions (<10 $e^{-}\cdot Å^{-2}$) with defocus values between 1.2 and 2.5 µm on a Tecnai 12 LaB6 electron microscope at 120 kV accelerating voltage using CCD Camera Gatan Orius 1000. The stain was Sodium Silico Tungstate $Na_4O_{40}SiW_{12}$ at 1% in distilled water (pH 7-7.5).

Isolation of membrane-bound TA for NMR analysis

WT cells grown in BHI to OD_{600} 0.8 were harvested by centrifugation (20 min, 4,500 *g*) and resuspended in 10 mL of 50 mM Tris-HCl pH 8, 150 mM NaCl, 5 mM $MgCl_2$ with 10 µg·mL^{-1} each of RNAse and DNAse, 9 µg·mL^{-1} mutanolysine, 50 µg·mL^{-1} lysozyme. After overnight incubation on a rotating wheel at 20°C, the lysate was centrifuged for 10 min at 15,000 *g*. The pellet was washed thrice with 5 mL water and thrice with 3 mL 100 mM ammonium acetate pH 4.2. The pellet was resuspended in 2.5 mL of the same buffer and 2.5 mL of water-saturated butanol. After vigorous mixing for 30 min, phases were separated by centrifugation at 3,220 *g* for 10 min. The butanol phase was reextracted twice with 2.5 mL water. The aqueous phases were combined and extracted with 8 mL and then 2 mL $CHCl_3$. The resulting combined chloroform phases was reextracted with 4 mL water. All water phases were combined and lyophilized. One half of the sample was dissolved in 200 µL of D_2O for NMR analysis. The other half of the sample was dissolved in 500 µL hydrazine 64% and incubated at room temperature for 4 h prior to addition of 500 µL acetone. The sample was dried under nitrogen flow, dissolved in 500 µL acetone and dried again. After dissolution in 200 µL D_2O and removal of insoluble material by centrifugation at 20,000 *g* for 10 min, the hydrazinolized sample was analyzed by NMR.

NMR analysis

NMR experiments were recorded on 600 and 700 MHz spectrometers equipped with a 5 mm TCI probe at 50°C. ^{13}C-^{1}H HSQC (constant time) and 2D ^{13}C-edited ^{1}H-^{1}H total correlated spectroscopy (TOCSY) were used to confirm ^{1}H-^{13}C assignment. ^{31}P 1D experiment was recorded with ^{1}H decoupling during acquisition and a recycling delay of 1 second. Data were processed with TopSpin 3.5 (Bruker) and analyzed with CcpNmr 2.5.

674

675 **Titration of cellular TA**

676 A preculture of WT cells in BHI was washed twice with C-medium without choline prior to
677 inoculating a C-medium culture containing 200 µM aCho at an OD_{600} of 0.06. After incubation at 37°C,
678 cells were harvested when the OD_{600} reached 0.265, that is after more than two generations in C-
679 medium.

680 Cells from 10 mL culture were resuspended in 160 µL of 50 mM Tris-HCl pH 8, 150 mM NaCl,
681 8 mM $MgCl_2$ containing 0.4 mg·mL^{-1} lysozyme, 0.3 mg·mL^{-1} mutanolysine, 0.3 mg·mL^{-1} recombinant
682 pneumococcal LytA, and 0.4 mg·mL^{-1} each of RNase and DNase. The suspension was left on wheel
683 overnight at room temperature to allow complete lysis.

684 Considering that a cell suspension at an optical OD_{600} of 1 contains about $3.33 \cdot 10^8$ cells mL^{-1}, the
685 cell concentration of the lysate was about $5.52 \cdot 10^8$ mL^{-1}. The concentration of the stock solution of
686 DBCO-AF488 was determined by its absorbance at 494 nm using $\varepsilon = 73000$ M^{-1}·cm^{-1} to be 93 ± 5 µM
687 (sd).

688 The cell lysate and dilutions thereof were mixed with an equal volume of DBCO-AF488 in 50
689 mM Tris-HCl pH 8, 150 mM NaCl to final concentrations of 3.7 ± 0.2 and 1.9 ± 0.1 µM of DBCO-
690 AF488 and a maximum of $2.8 \cdot 10^8$ cells mL^{-1}. After 24 h of incubation at room temperature, 1 µL of
691 100 mM aCho were added to block unreacted DBCO-AF488 and incubation was continued for 2 h.

692 Samples were then analyzed by electrophoresis on polyacrylamide gel (17%, acrylamide:bis-
693 acrylamide 29:1) in the presence of 1% SDS with a Tris/tricine buffer system. The gels were imaged
694 by trans-illumination with UV light without saturation on a BioRad Chemidoc imager. Band intensities
695 were quantified using ImageJ.

696 **TA characterization at different stages of cell culture**

697 WT and Δ*lytA* cells were grown for over two generations in chemically defined medium (C-
698 medium) devoid of choline but supplemented with 200 µM aCho over two generations. Cells were
699 harvest during the exponential phase of growth at an OD_{600} of 0.38, at the onset of the stationary phase
700 at the OD_{600} of 0.75, and when the WT cells started to lyse (OD_{600} 0.46). TA were labeled and cell were
701 lysed, LTA and WTA were separated by centrifugation and analyzed by electrophoresis as described
702 above.

703 **TA pulse and pulse-chase labeling**

704 Exponentially growing WT cells in C-medium were harvested and resuspended at an OD_{600} of 8
705 in the same medium containing 200 µM aCho and no choline. After 0, 2, 5 and 10 min, 150 µL aliquots
706 were withdrawn, immediately centrifuged for 30 s at 10,000 *g* and resuspended in the same volume of
707 50 mM Tris-HCl pH 8, 150 mM NaCl. The washing procedure was repeated once prior to lysis,

secondary fluorescent click-labeling and fractionation as above. Pellets containing LTA were resuspended in one-eighth volume for concentration. TA were analyzed by gel electrophoresis as above.

Hydrolysis of sedimented TA from Δ*tacL* cells

Three procedures were tested. First, pellets of labeled lysates of WT or Δ*tacL* cells were resuspended in solutions of 150 mM NaCl buffered with either 50 mM Tris-HCl pH 8 or ammonium acetate pH 4.2, and incubated for 3 h at room temperature or 110°C.

Secondly, the LTA isolation procedure of Hess and colleagues (24) was applied. Labeled pellets resulting from 10 mL of culture of Δ*tacL* or 7 mL of WT cells were dissolved in 200 µL of 50 mM sodium citrate pH 4.7, 4% SDS and incubated at 100°C for 45 min. After withdrawal of a 20 µL aliquot for analysis, the solution was lyophilized. The solid was washed four times with ethanol and resuspended in 180 µL of 50 mM sodium citrate pH 4.7. A second 20 µL aliquot was withdrawn, and the solution was extracted with 150 µL water-saturated butanol. The organic phase was back extracted with 100 µL water. The aqueous phases were combined, lyophilized, redissolved in 160 µL of 50 mM sodium citrate pH 4.7, and a 20 µL aliquot was taken for analysis. To the 20 µL aliquots, 2 µL of 3 M Tris-HCl pH 8.45 were added prior to analysis by electrophoresis.

Thirdly, recombinant colicin M from *P. aeruginosa* (generous gift from T. Touzé) prepared as described previously (43), was added at various concentrations to resuspended pellets and the mixtures were incubated overnight at room temperature.

References

1. S. Brown, J. P. Santa Maria, S. Walker, Wall teichoic acids of gram-positive bacteria. *Annu. Rev. Microbiol.* **67**, 313–336 (2013).

2. D. Denapaite, R. Brückner, R. Hakenbeck, W. Vollmer, Biosynthesis of teichoic acids in Streptococcus pneumoniae and closely related species: lessons from genomes. *Microb. Drug Resist. Larchmt. N* **18**, 344–358 (2012).

3. M. G. Percy, A. Gründling, Lipoteichoic acid synthesis and function in gram-positive bacteria. *Annu. Rev. Microbiol.* **68**, 81–100 (2014).

4. J. Dubochet, *et al.*, Cryo-electron microscopy of vitrified specimens. *Q. Rev. Biophys.* **21**, 129–228 (1988).

5. V. R. F. Matias, T. J. Beveridge, Cryo-electron microscopy of cell division in Staphylococcus aureus reveals a mid-zone between nascent cross walls. *Mol. Microbiol.* **64**, 195–206 (2007).

6. V. R. F. Matias, T. J. Beveridge, Lipoteichoic acid is a major component of the Bacillus subtilis periplasm. *J. Bacteriol.* **190**, 7414–7418 (2008).

7. B. Zuber, *et al.*, Granular layer in the periplasmic space of gram-positive bacteria and fine structures of Enterococcus gallinarum and Streptococcus gordonii septa revealed by cryo-electron microscopy of vitreous sections. *J. Bacteriol.* **188**, 6652–6660 (2006).

8. H. P. Erickson, How Teichoic Acids Could Support a Periplasm in Gram-Positive Bacteria, and Let Cell Division Cheat Turgor Pressure. *Front. Microbiol.* **12**, 664704 (2021).

9. B. Maestro, J. M. Sanz, Choline Binding Proteins from Streptococcus pneumoniae: A Dual Role as Enzybiotics and Targets for the Design of New Antimicrobials. *Antibiot. Basel Switz.* **5** (2016).

10. A. Tomasz, Choline in the cell wall of a bacterium: novel type of polymer-linked choline in Pneumococcus. *Science* **157**, 694–697 (1967).

11. E. Badger, The Structural Specificity of Choline for the Growth of Type Iii Pneumococcus. *J. Biol. Chem.* **153**, 183–191 (1944).

12. H. Laitinen, A. Tomasz, Changes in composition of peptidoglycan during maturation of the cell wall in pneumococci. *J. Bacteriol.* **172**, 5961–5967 (1990).

13. A. M. Di Guilmi, *et al.*, Specific and spatial labeling of choline-containing teichoic acids in Streptococcus pneumoniae by click chemistry. *Chem. Commun. Camb. Engl.* **53**, 10572–10575 (2017).

14. J. Bonnet, *et al.*, One-Pot Two-Step Metabolic Labeling of Teichoic Acids and Direct Labeling of Peptidoglycan Reveals Tight Coordination of Both Polymers Inserted into Pneumococcus Cell Wall. *ACS Chem. Biol.* **13**, 2010–2015 (2018).

15. W. Fischer, Pneumococcal lipoteichoic and teichoic acid. *Microb. Drug Resist. Larchmt. N* **3**, 309–325 (1997).

16. N. Gisch, *et al.*, Structural reevaluation of Streptococcus pneumoniae Lipoteichoic acid and new insights into its immunostimulatory potency. *J. Biol. Chem.* **288**, 15654–15667 (2013).

17. N. K. Bui, *et al.*, Isolation and analysis of cell wall components from Streptococcus pneumoniae. *Anal. Biochem.* **421**, 657–666 (2012).

18. M. Damjanovic, A. S. Kharat, A. Eberhardt, A. Tomasz, W. Vollmer, The Essential tacF Gene Is Responsible for the Choline-Dependent Growth Phenotype of Streptococcus pneumoniae. *J. Bacteriol.* **189**, 7105–7111 (2007).

19. X. Liu, *et al.*, High-throughput CRISPRi phenotyping identifies new essential genes in Streptococcus pneumoniae. *Mol. Syst. Biol.* **13**, 931 (2017).

20. P. S. Gibson, J.-W. Veening, Gaps in the wall: understanding cell wall biology to tackle amoxicillin resistance in *Streptococcus pneumoniae*. *Curr. Opin. Microbiol.* **72**, 102261 (2023).

21. V. Minhas, *et al.*, Competence remodels the pneumococcal cell wall exposing key surface virulence factors that mediate increased host adherence. *PLoS Biol.* **21**, e3001990 (2023).

22. Y. Kawai, *et al.*, A widespread family of bacterial cell wall assembly proteins. *EMBO J.* **30**, 4931–4941 (2011).

23. A. Eberhardt, *et al.*, Attachment of capsular polysaccharide to the cell wall in Streptococcus pneumoniae. *Microb. Drug Resist. Larchmt. N* **18**, 240–255 (2012).

24. N. Heß, *et al.*, Lipoteichoic acid deficiency permits normal growth but impairs virulence of Streptococcus pneumoniae. *Nat. Commun.* **8**, 2093 (2017).

25. J. Flores-Kim, G. S. Dobihal, T. G. Bernhardt, D. Z. Rudner, WhyD tailors surface polymers to prevent premature bacteriolysis and direct cell elongation in Streptococcus pneumoniae. *eLife* **11**, e76392 (2022).

26. V. R. F. Matias, T. J. Beveridge, Cryo-electron microscopy reveals native polymeric cell wall structure in Bacillus subtilis 168 and the existence of a periplasmic space. *Mol. Microbiol.* **56**, 240–251 (2005).

27. J. Trouve, O. Glushonkov, C. Morlot, Metabolic biorthogonal labeling and dSTORM imaging of peptidoglycan synthesis in Streptococcus pneumoniae. *STAR Protoc.* **2**, 101006 (2021).

28. J. Trouve, *et al.*, Nanoscale dynamics of peptidoglycan assembly during the cell cycle of Streptococcus pneumoniae. *Curr. Biol. CB* **31**, 2844-2856.e6 (2021).

29. J. Flores-Kim, G. S. Dobihal, A. Fenton, D. Z. Rudner, T. G. Bernhardt, A switch in surface polymer biogenesis triggers growth-phase-dependent and antibiotic-induced bacteriolysis. *eLife* **8**, e44912 (2019).

30. Y. Higashi, J. L. Strominger, C. C. Sweeley, Structure of a lipid intermediate in cell wall peptidoglycan synthesis: a derivative of a C55 isoprenoid alcohol. *Proc. Natl. Acad. Sci. U. S. A.* **57**, 1878–1884 (1967).

31. D. Chérier, D. Patin, D. Blanot, T. Touzé, H. Barreteau, The Biology of Colicin M and Its Orthologs. *Antibiotics* **10**, 1109 (2021).

32. H. Barreteau, *et al.*, Human- and Plant-Pathogenic Pseudomonas Species Produce Bacteriocins Exhibiting Colicin M-Like Hydrolase Activity towards Peptidoglycan Precursors. *J. Bacteriol.* **191**, 3657–3664 (2009).

33. S. J. Gould, R. C. Lewontin, The spandrels of San Marco and the Panglossian paradigm: a critique of the adaptationist programme. *Proc. R. Soc. Lond. B Biol. Sci.* **205**, 581–598 (1979).

34. O.-J. Park, *et al.*, Streptococcus gordonii: Pathogenesis and Host Response to Its Cell Wall Components. *Microorganisms* **8**, 1852 (2020).

35. B. P. Lima, *et al.*, Streptococcus gordonii Type I Lipoteichoic Acid Contributes to Surface Protein Biogenesis. *mSphere* **4**, e00814-19 (2019).

36. P. G. De Gennes, Polymers at an interface; a simplified view. *Adv. Colloid Interface Sci.* **27**, 189–209 (1987).

37. J. Bonnet, *et al.*, Nascent teichoic acids insertion into the cell wall directs the localization and activity of the major pneumococcal autolysin LytA. *Cell Surf.* **2**, 24–37 (2018).

38. B. De Las Rivas, J. L. García, R. López, P. García, Purification and polar localization of pneumococcal LytB, a putative endo-beta-N-acetylglucosaminidase: the chain-dispersing murein hydrolase. *J. Bacteriol.* **184**, 4988–5000 (2002).

39. S. Martínez-Caballero, *et al.*, Molecular basis of the final step of cell division in *Streptococcus pneumoniae*. *Cell Rep.* **42**, 112756 (2023).

40. P. Calvez, J. Jouhet, V. Vié, C. Durmort, A. Zapun, Lipid Phases and Cell Geometry During the Cell Cycle of Streptococcus pneumoniae. *Front. Microbiol.* **10** (2019).

41. D. Mastronarde, Tomographic Reconstruction with the IMOD Software Package. *Microsc. Microanal.* **12**, 178–179 (2006).

42. R. C. Valentine, B. M. Shapiro, E. R. Stadtman, Regulation of glutamine synthetase. XII. Electron microscopy of the enzyme from Escherichia coli. *Biochemistry* **7**, 2143–2152 (1968).

43. H. Barreteau, *et al.*, Functional and structural characterization of PaeM, a colicin M-like bacteriocin produced by Pseudomonas aeruginosa. *J. Biol. Chem.* **287**, 37395–37405 (2012).

836 # Figures and legends

837

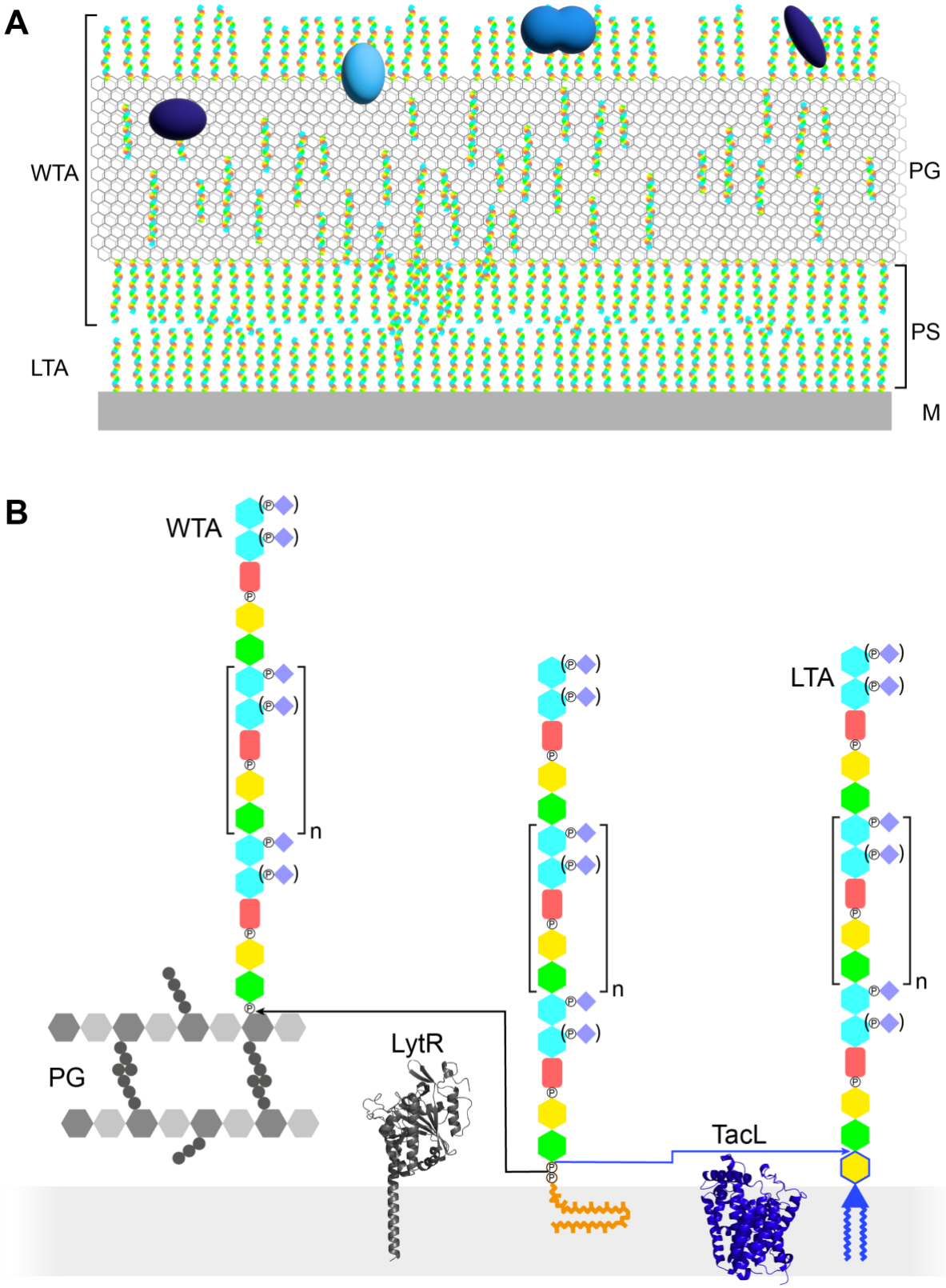

838

839

Figure 1. Models of the functions and structures of TA in *S. pneumoniae*. (**A**) TA (multicolored rods) attached to the membrane (M) or to the peptidoglycan (PG) exclude each other to maintain a periplasmic space (PS). Additional functions arise from the presentation of various choline-binding proteins (blue). (**B**) Polymerized TA attached to undecaprenyl (UndPr)-pyrophosphate are transferred at the cell surface onto PG by the phosphotransferase LytR to form WTA; or onto DGlc*p*-DAG by TacL to form LTA. The enzymes are depicted by their AlphaFold models. The most abundant TA species have 6 repeating units (n = 4).

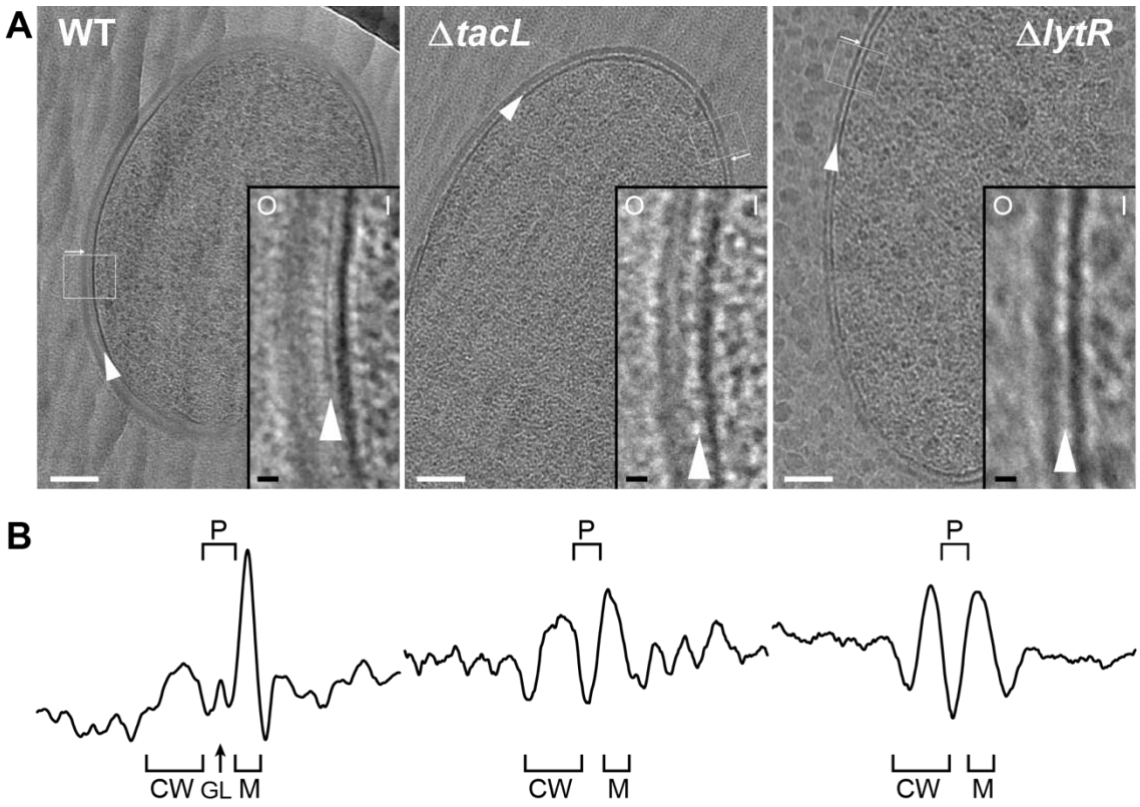

Figure 2. Electron micrographs of WT, Δ*tacL* and Δ*lytR* strains. (**A**) CEMOVIS micrographs allowing full view (white scale bar, 100 nm) and zoom (black scale bar, 10 nm) of WT and mutant strains. O and I signal the outer and inner sides of the cell envelope. A periplasmic space can be observed in all three strains. A granular layer is seen as a thin black line in the periplasmic space (arrowheads) of WT cells, whereas it is not observed in the Δ*lytR* and Δ*tacL* strains. (**B**) Corresponding pixel intensity profile of the cell envelope is shown for each strain. The intensity profiles were measured perpendicularly to the cell surface in regions boxed in white, and show variations in the density of the envelope ultrastructure. CW, cell wall; P, periplasm; GL, granular layer; M, membrane.

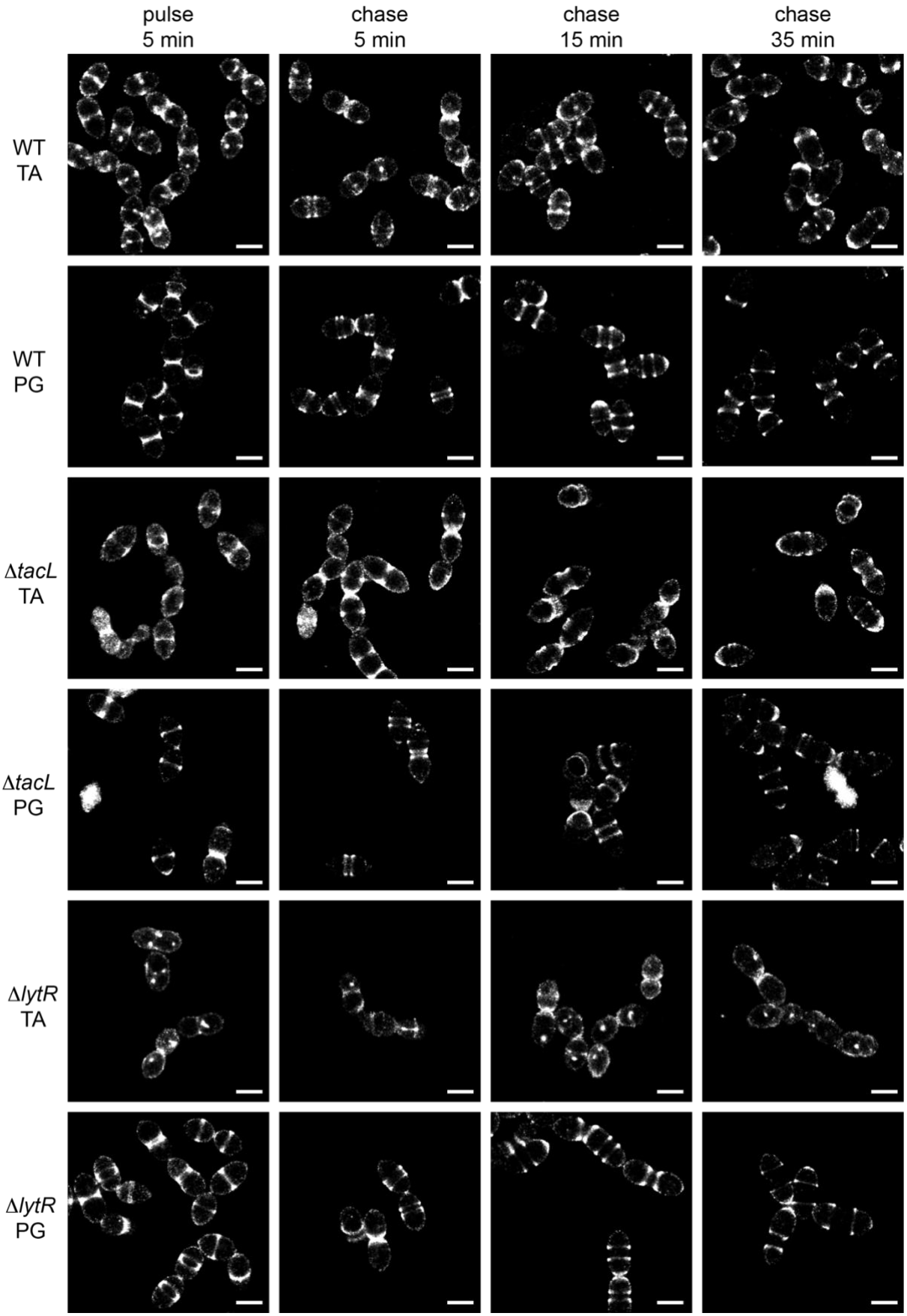

859
860

Figure 3. Super-resolved dSTORM imaging of TA incorporated in growing WT, Δ*tacL* and Δ*lytR* cells after a 5 min pulse of metabolic labeling with 1.5 mM aCho followed by a chase, and subsequent secondary fluorescent labeling by click chemistry using DBCO-AF647. For comparison, the same pulse-chase procedure was applied to reveal the newly synthesized peptidoglycan (PG) with a metabolic labeling using 2 mM azido-D-Ala-D-Ala. Scale bars are 1 µm. Corresponding conventional and bright field images are shown in SI **Fig. S5A**.

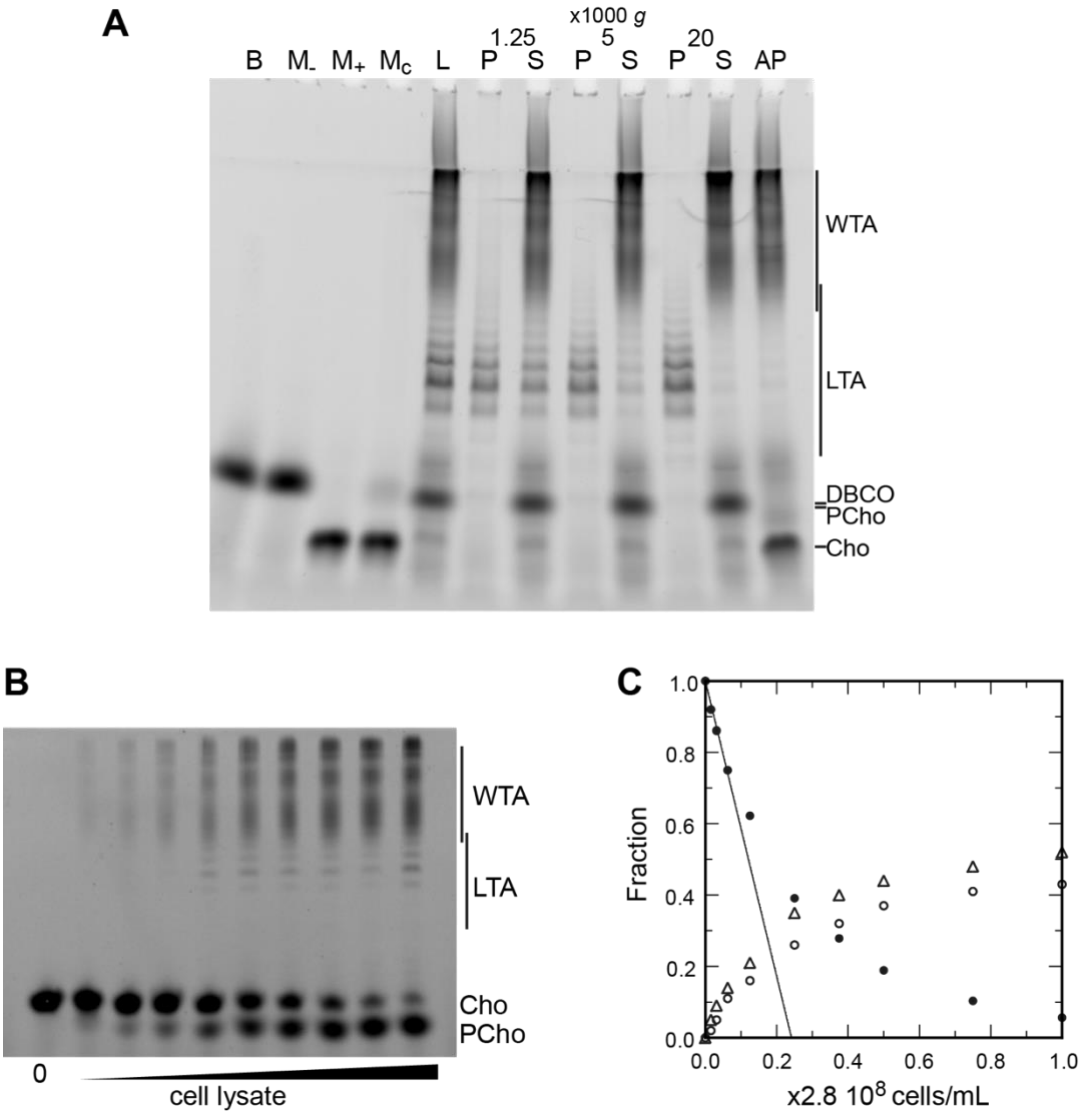

868
869

Figure 4. (**A**) Polyacrylamide gel electrophoresis of fluorescently labeled TA demonstrating separation of LTA and WTA by centrifugation. Labeled compounds were revealed by UV-transillumination. TA were labeled by growing WT cells in C-medium in the presence of 200 µM aCho. Cells were lysed overnight with lysozyme, mutanolysine and LytA and the azido-groups were modified by reaction with 25 µM DBCO-AF488. The lysate was centrifuged for 2 min at 1,250, 5,000 or 20,000 *g*. The pellets were resuspended in the initial volume. An aliquot of the 20,000 *g* supernatant was treated with alkaline phosphatase. The buffer with the lysing enzymes, the medium with and without aCho and the culture supernatant were similarly incubated with 25 µM DBCO-AF488. B, lysis buffer with enzymes; M-, C-medium without aCho; M+, C-medium with aCho; M_C, culture supernatant; L, lysate; P, pellet; S, supernatant; AP, alkaline phosphatase-treated. The control samples (B, M-, M+ and M_C were loaded at one-fourth the volume of the cellular samples). Labels on the right side of the gel identify species coupled to the fluorophore AF488. (**B-C**) Titration of cellular TA. WT cells were grown for two generation in the presence of aCho prior to cell lysis. DBCO-AF488 (1.9 µM) was incubated for 24 h with varying amounts of cell lysate corresponding to up to 2.9 10^8 cells mL^{-1}. The remaining DBCO-AF488 was blocked by addition of 100 mM aCho, and the various species were separated by polyacrylamide (17%) gel electrophoresis (**B**). The bands were quantified and the relative amount of the various species were plotted against the cell concentration (**C**). Black circles, blocked DBCO-AF488; open circle, phosphocholine; open triangle, TA. A linear regression of the DBCO-AF488 points at low cellular concentration was applied to obtain the titration point as the intercept of the cell concentration axis.

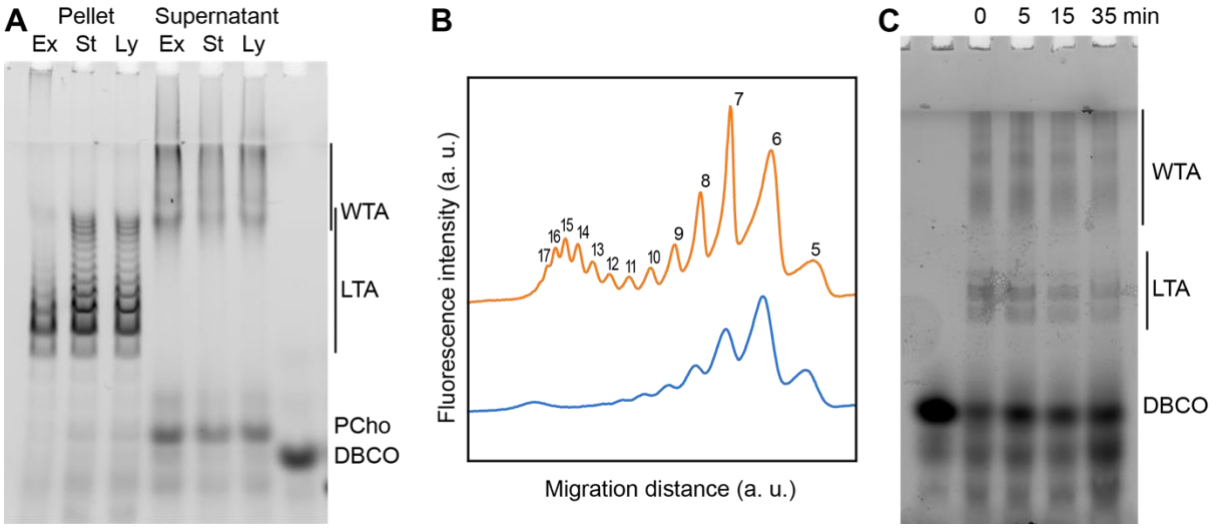

Figure 5. Evolution of TA during growth phases. (**A**) WT cells grown in C-medium containing 200 µM aCho were harvested during the exponential growth phase (Ex), at the onset of the stationary phase (St) and during the autolysis (Ly). TA were fluorescently click-labeled with DBCO-AF488 and cells were completely lysed by the addition of PG hydrolases prior to centrifugation. LTA are found in the pellet (P) whereas WTA are observed in the supernatant (S). The amounts of cells at the different culture stages were normalized. The LTA samples are 8-fold concentrated compared to the WTA samples. Fluorescently labeled TA were revealed by UV-transillumination after SDS-polyacrylamide electrophoresis. (**B**) Densitometric profiles of the fluorescent intensities of exponential (blue) and stationary phase samples (orange) shown in (**A**). (**C**) Electrophoretic analysis of TA of WT cells grown in BHI and pulse-labeled for 5 min with 1.5 mM aCho, and chased by further growth in the same medium without added aCho for the indicated duration.

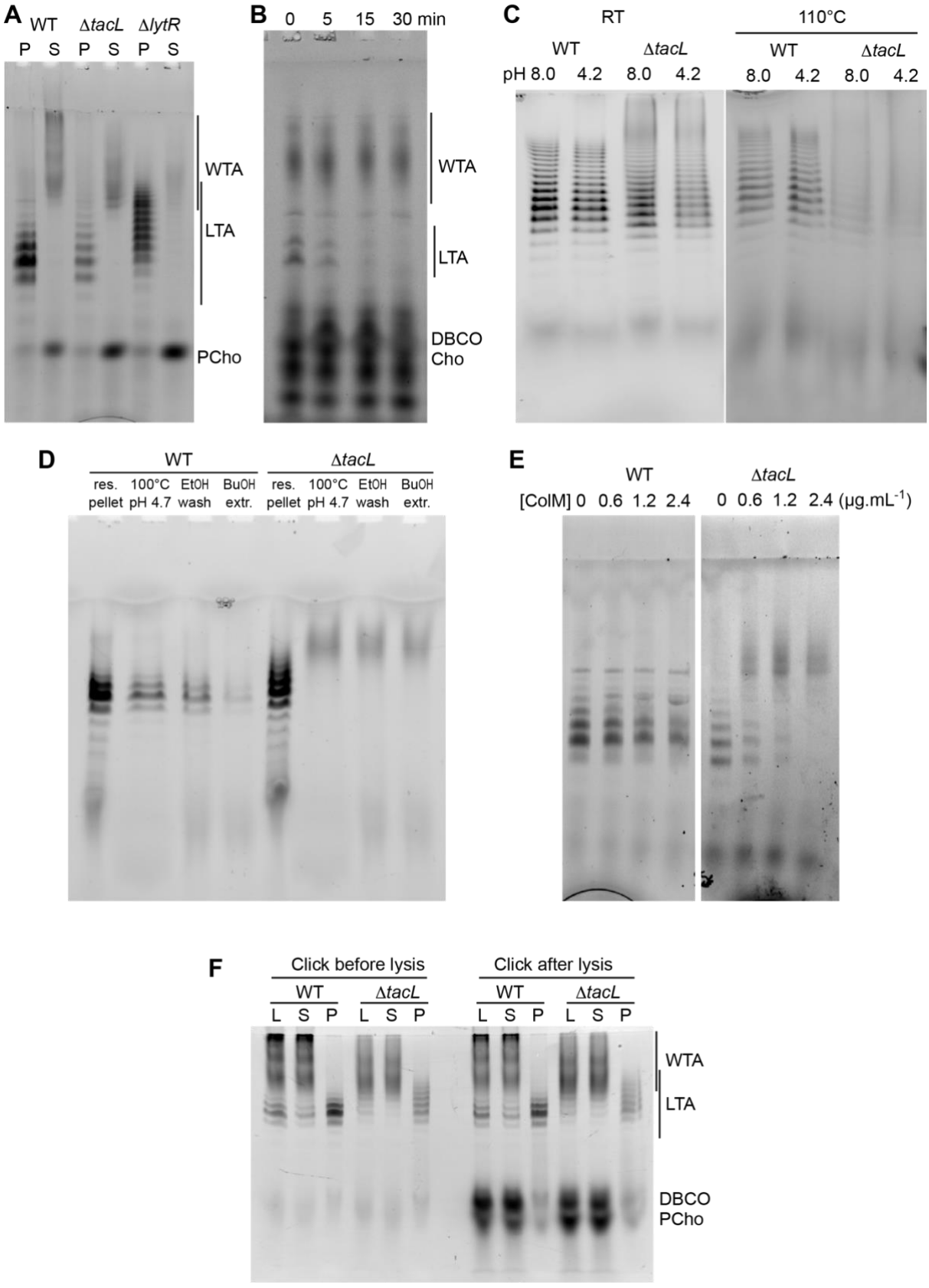

Figure 6. (**A**) Electrophoretic analysis of TA from the WT strain, or deleted of the gene encoding the glycosyltransferase TacL, or the phosphotransferase LytR. Cells were grown in C-medium with no choline and 200 µM aCho, prior to cell lysis with PG hydrolases and secondary labeling with DBCO-AF488. Lysates were fractionated by centrifugation and the pellets were resuspended in one fourth the initial volume: P, pellet; S, supernatant. (**B-E**) Identification of sedimented TA from lysates of Δ*tacL* cells as undecaprenyl-pyrophosphate bound precursors. (**B**) Pulse-chase labeling experiment of TA in strain Δ*tacL*. Cells grown in BHI were exposed to 1.5 mM aCho for 10 min (pulse), prior to washing and further incubation in the same media without aCho (chase) for various time prior to cell lysis and secondary labeling with DBCO-AF488. Samples were treated with alkaline phosphatase prior to electrophoresis. (**C**) Pellets containing labeled TA from WT and Δ*tacL* cells were resuspended in a Tris- or ammonium acetate-buffered solution at pH 8 or pH 4.2 and incubated for 3 h at room temperature or 110°C prior to electrophoresis. (**D**) Labeled TA from WT and Δ*tacL* cells were submitted to the first steps of the traditional procedure of LTA isolation: boiling in 4% SDS in a citrate-buffered solution at pH 4.7, lyophilization and ethanol wash of the lyophilizate, butanol extraction and retention of the aqueous fraction. (**E**) Labeled sedimented TA from WT and Δ*tacL* cells were incubated overnight without or with various concentrations of recombinant *P. aeruginosa* colicin M prior to electrophoretic separation. (**F**) To probe on which side of the plasma membrane the TA are positioned, secondary click-labeling with DBCO-AF488 was performed prior or after cell lysis of WT and Δ*tacL* cells grown in C-medium in the presence of 0.2 mM azido-choline. L, whole lysate; S, supernatant of 20,000 *g* 2 min centrifugation; P, pellet resuspended in one-fourth initial volume.

Table 1

Table 1. Dimensions of cell envelope structures measured on CEMOVIS images

Strain	Mean thickness (nm) ± SD (nb of measurements) [a]			Ratio of thickness PG/PS	GL dist. from membrane [b] (nm)± SD
	PG layer	PS	GL		
WT	15.9 ± 2.5 (35)	10.8 ± 1.4 (35)	3.2 ± 0.8 (35)	1.5	5.0 ± 0.8 (35)
Δ*tacL*	13.3 ± 3.7 (35) [c] **/ [d] **	7.1 ± 2.3 (35) [c] **/[d] #	NA	1.87 [c] **/ [d] **	NA
Δ*lytR*	10.2 ± 1.7 (35) [c] **/ [d] **	7.7 ± 2.0 (35) [c] **/[d] #	NA	1.32 [c] #/[d] **	NA

[a] Values in nm are presented as mean values ± standard deviations (with numbers of measurements in parentheses). They have been measured using images with a pixel size of 3.7 Å. NA, not applicable.

[b] Measured from the outer surface of the cytoplasmic membrane to the inner most side of the GL.

[c] Anova test was performed between corresponding structures of WT R800 and mutant cells. #, no statistical difference; *, p= 0.05; **, p= 0.01

[d] Anova test was performed between corresponding structures of Δ*lytR* and Δ*tacL* cells. #, no statistical difference; *, p= 0.05; **,p = 0.01.

Table 2

Table 2. *S. pneumoniae* strains used in this study

Short name	Construct	Genotype	Source
WT	sspCM514	R800, *rpsL1*, StrR	Gift from J.-P. Claverys, Toulouse, France
Δ*tacL*	sspCM246	R800, *rpsL1*, Δ*tacL*, StrR	This study
Δ*lytR*	sspCM493	R800, *rpsL1*, Δ*lytR*, StrR	This study

934 **SUPPLEMENTARY INFORMATION**

935

936 # Teichoic acids in the periplasm and the cell envelope of

937 # *Streptococcus pneumoniae*

938

939 Mai Nguyen[a], Elda Bauda[a], Célia Boyat[a], Cédric Laguri[a], Céline Freton[a], Anne Chouquet[a], Benoit
940 Gallet[a], Morgane Baudoin[b], Yung-Sing Wong[b], Christophe Grangeasse[c], Christine Moriscot[c], Claire
941 Durmort[a], André Zapun[a] & Cecile Morlot[a]

942 [a]Univ. Grenoble Alpes, CNRS, CEA, IBS, F-38000 Grenoble, France

943 [b]Univ. Grenoble Alpes, CNRS, DPM, UMR5063, 38000 Grenoble, France

944 [c]Molecular Microbiology and Structural Biochemistry, Université de Lyon, CNRS, UMR5086, 69007
945 Lyon, France

946

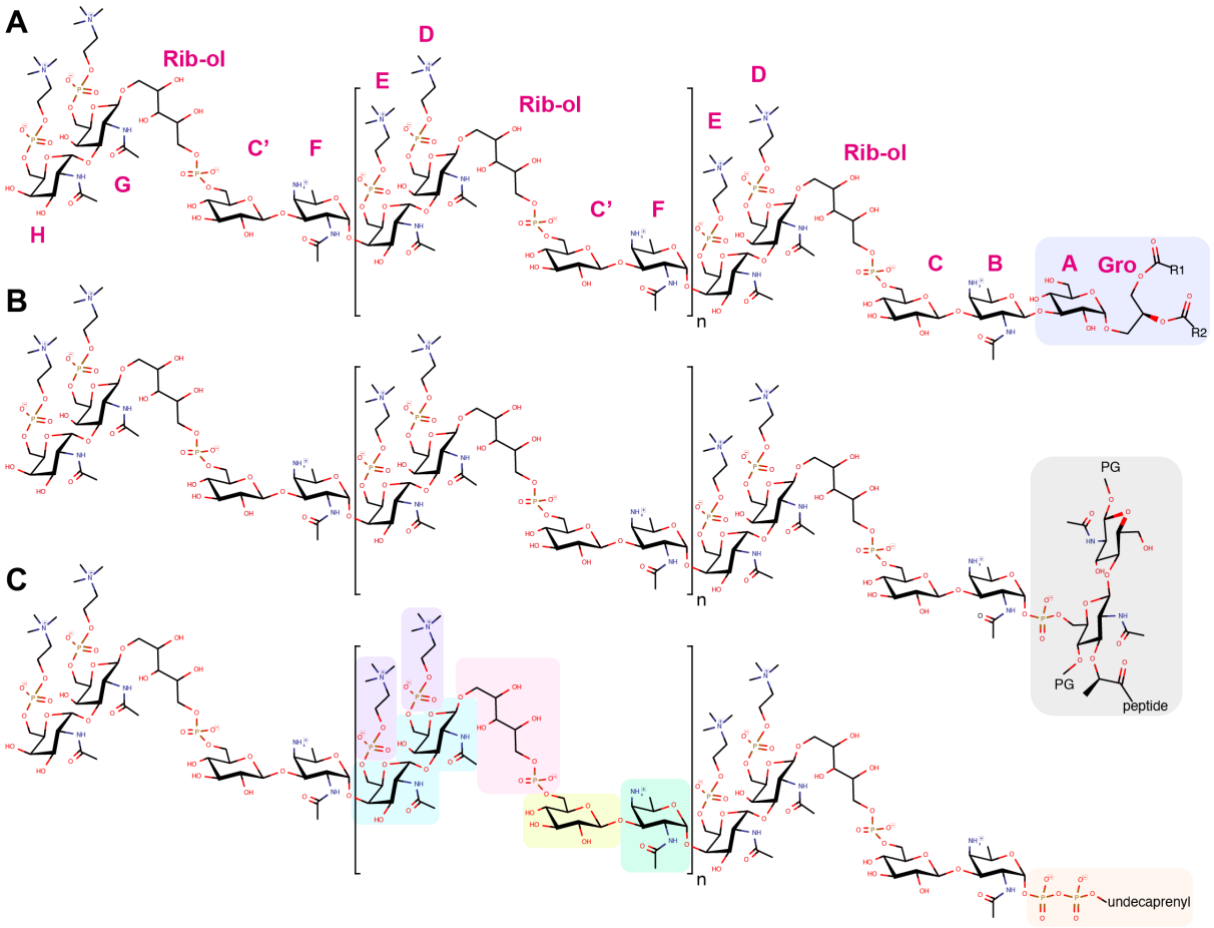

Figure S1. Chemical structure of (**A**) LTA, (**B**) WTA, and (**C**) the membrane-bound precursor. The constituent of the repeating unit are in green the acetamido-4-amino-6-deoxygalactopyranose (AATGal*p*NAc), in yellow the glucopyranose (DGlc*p*), in pink the ribitol-5-phosphate, in cyan the N-acetylgalactosamine (DGal*p*NAc), in purple the phosphocholine. One or both phosphocholine residues can be absent on the terminal unit. Some units may also lack the phosphocholine on the proximal DGal*p*NAc. The most abundant species have 6 repeating units (n=4). LTA are β-1-liked to monoglucosyldiacylglycerol (blue). WTA are α-1-linked via a phosphodiester to position 6 of a N-acetyl muramic acid of the peptidoglycan (PG, gray). The precursors remain attached to an undecaprenyl pyrophosphate (orange). The one-letter nomenclature of constituents proposed by Gisch (1) is given in magenta around the LTA.

Notes on CEMOVIS data quality.

Some crevasses can be observed but the section is devoid of cracks and very low ice contamination is present on the surface (SI **Fig. S2**). Knife marks along the cutting direction of the knife cannot be avoided, although compression artifact is rather limited as the cells preserve a round shape. Thus, it can be said reasonably that the sections are exploitable and that artifacts induced by cryo-sectioning do not impair image interpretation and ultrastructure measurement.

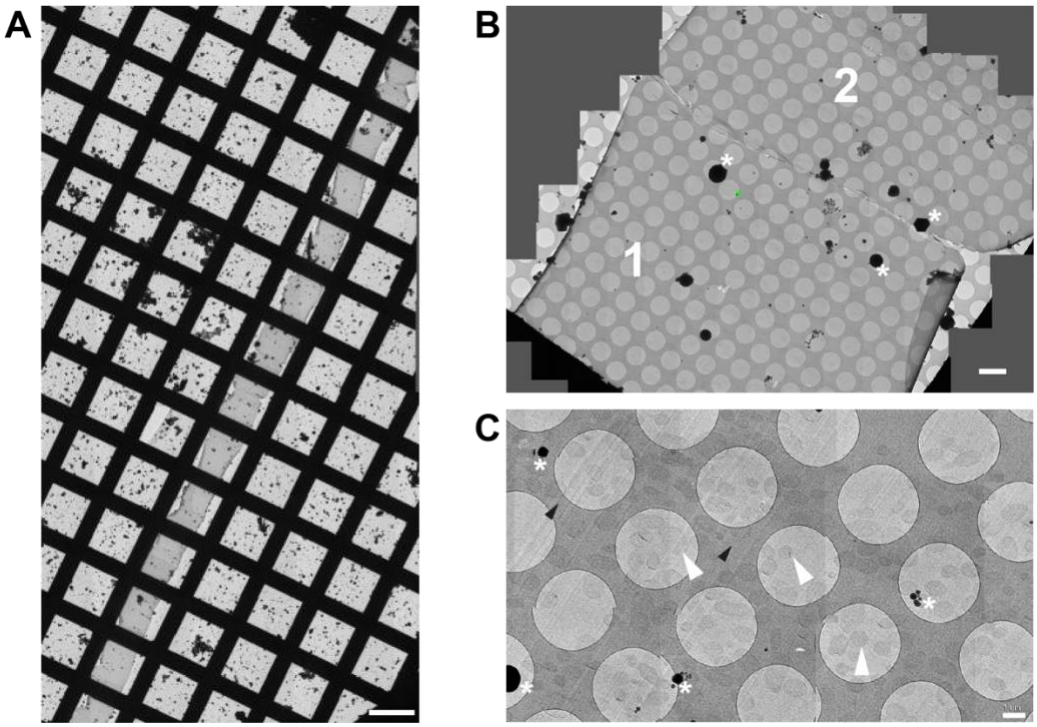

Figure S2. Low-magnification CEMOVIS images of *S. pneumoniae* Δ*tacL*. (**A**) The ribbon spans the entire EM grid. Scale bar, 100 µm. (**B**) Stitching of several acquisitions areas showing one cryo-section (1) and half of a second one (2) inside the ribbon. Scale bar, 5 µm. (**C**). Cells are uniformly distributed in the section. Representative acquisition areas, where cells are located at the center of a hole in the carbon, are pointed with a white arrowhead. Scale bar, 1 µm. Black arrowheads: knife marks; asterisks: ice contamination.

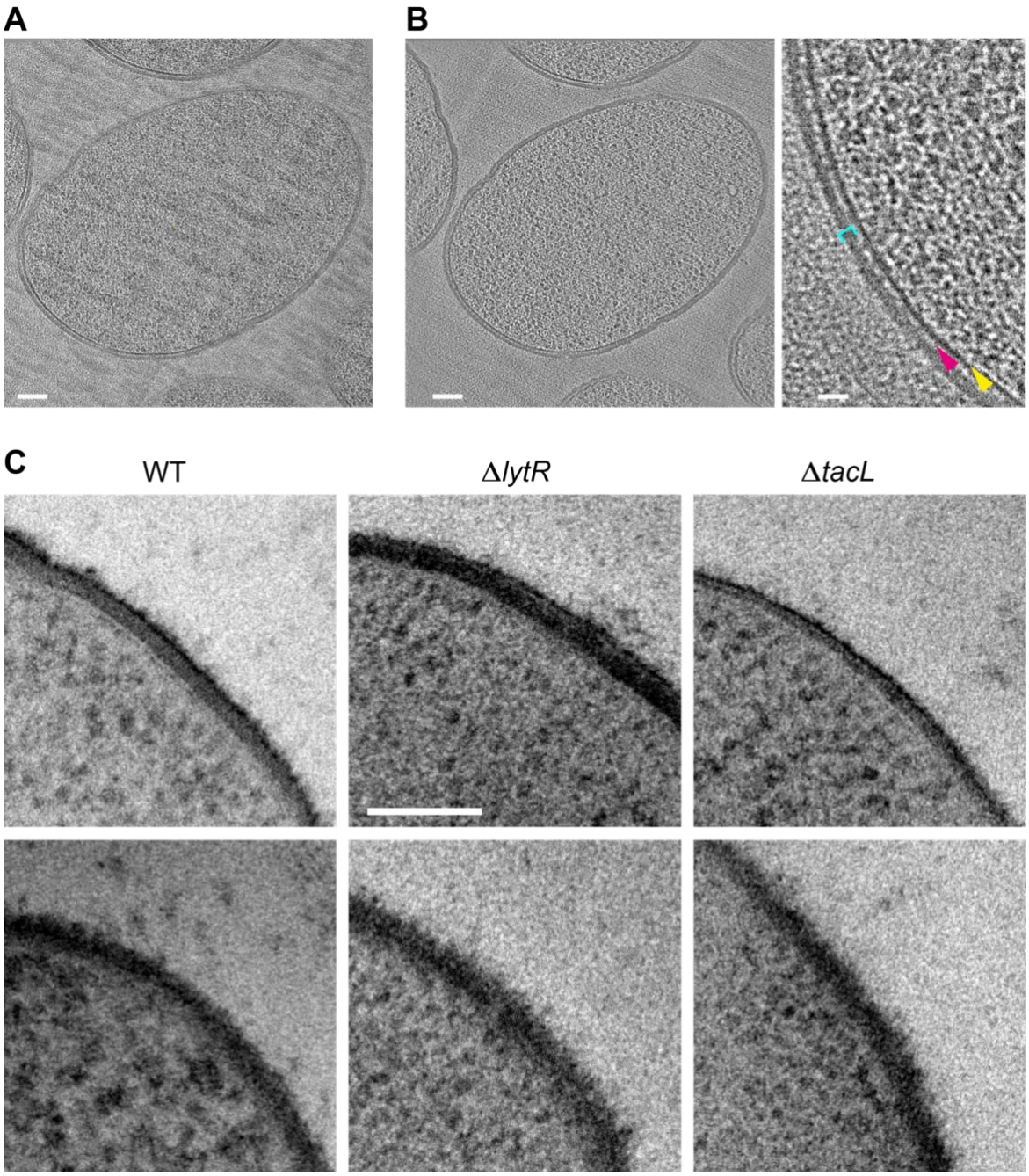

Figure S3. (**A**-**B**) CETOVIS of a Δ*tacL* cell section. (**A**) Raw image of a tilt series. (**B**) Full view (scale bar, 100 nm) and zoom (scale bar, 20 nm) of a slice through the cryo-electron tomogram. Yellow arrow, membrane; magenta arrow; periplasmic space; cyan bracket, peptidoglycan. The reduction of the periplasmic space and peptidoglycan layers thickness is observed in the whole volume. No granular layer is detected in the volume. (**C**) TEM micrographs of stained freeze-substituted thin sections of the cell envelope of WT, Δ*lytR* and Δ*tacL* cells. The appearance varies depending on the angle between the cell envelope and the section plane. Two examples are shown for each strain. No consistent difference could be discerned between the strains. Scale bar 100 nm.

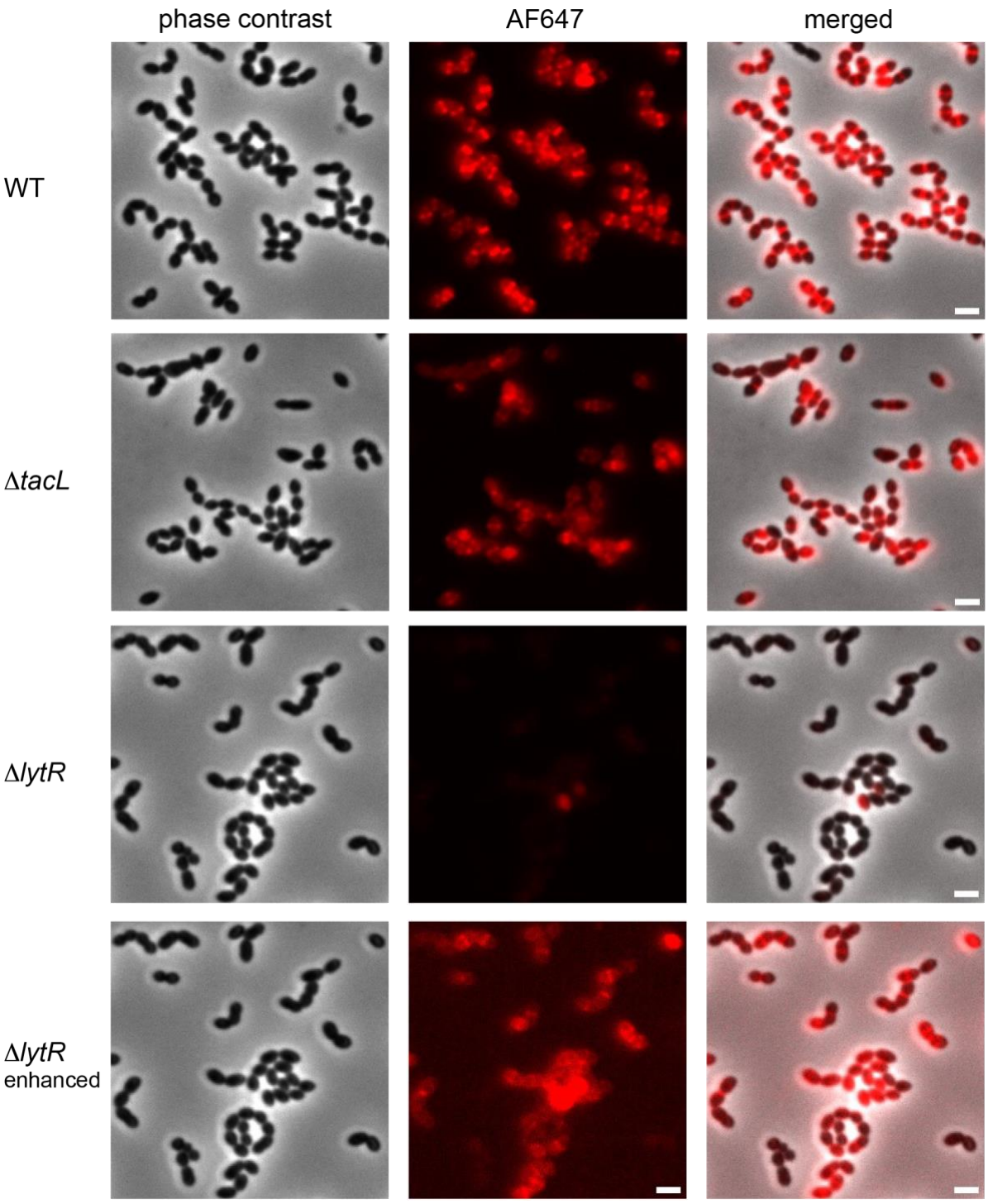

Figure S4. Fluorescence microscopy of R800 WT, Δ*tacL* and Δ*lytR* cells grown in BHI and pulse-labeled with 1.5 mM azido-choline for 5 min prior to fixation and secondary click-labeling with DBCO-AF647. The three top rows are with the same imaging settings. The fluorescent signal of the bottom row was enhanced. Scale bars are 2 µm.

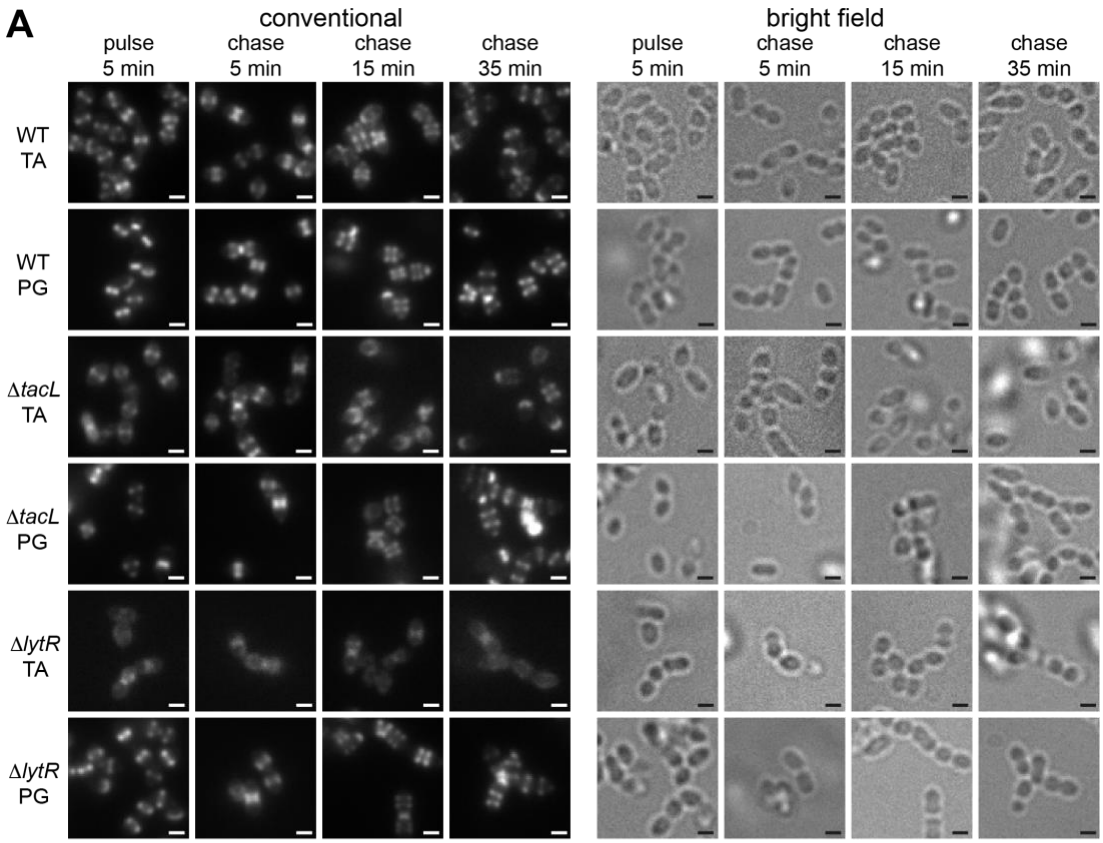

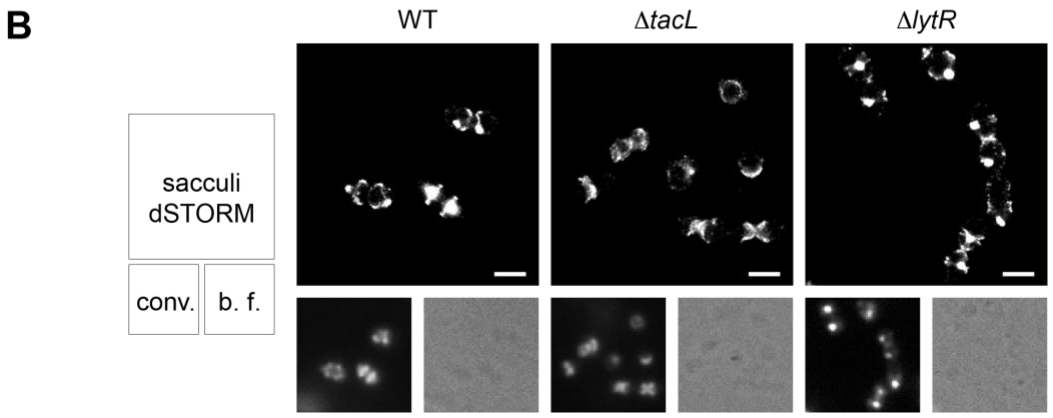

990

991 **Figure S5.** (**A**) Corresponding conventional and bright field microscopy images of the pulse-chase
992 experiments shown by dSTORM imaging in **Fig. 3**. New TA were revealed in growing R800 WT, Δ*tacL*
993 and Δ*lytR* cells by a 5 min pulse of metabolic labeling with 1.5 mM azido-choline followed by a chase,
994 and subsequent secondary fluorescent labeling with clickable DBCO-AF647. For comparison, the same
995 pulse-chase procedure was applied to reveal the new peptidoglycan with a metabolic labeling using 1.5
996 mM azido-D-Ala-D-Ala. (**B**) dSTORM imaging (with corresponding conventional and bright field
997 images at half scale) of sacculi prepared from cells pulse-labeled during 5 min and chased for 15 min.
998 Labeled TA in sacculi were revealed by secondary fluorescent labeling with clickable DBCO-AF647.
999 Scale bars are 1 µm.

Notes on the fractionation of LTA and WTA

Although sedimentation of LTA was observed even at relative centrifugal force as low as 2,000 *g*, the pelleting was not always complete, even after prolonged centrifugation at 20,000 *g*. Incomplete cell lysis cannot account for the incomplete pelleting of LTA, since intact cells or large fragments would be expected to add to the pellet material. We found out that the quality of the separation of LTA from solubilized WTA by sedimentation depended on the amount of recombinant LytA used during the lysis (SI **Fig. S6**). This parameter was difficult to adjust since the exactly adequate amount appeared to depend on the particulars of the experiment (strain, cell density). We think that the multivalent choline-binding domain of LytA crosslinks LTA bounds to membrane vesicles, leading to the formation of large aggregates that sediment more easily. In support of this explanation, the presence recombinant LytA also impacts the migration of the solubilized TA, causing species with lower electrophoretic mobilities to be more abundant at the top of the gels.

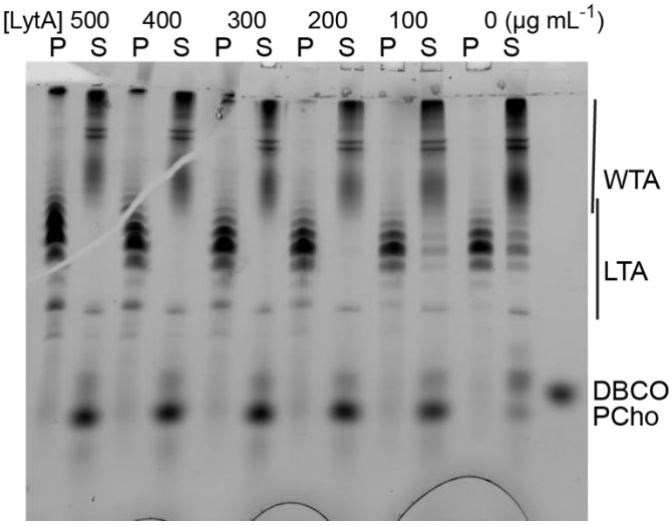

Figure S6. Effect of the concentration of added recombinant LytA on the sedimentation of LTA. R800 WT cells grown in C-medium with 200 µM azido-choline were click-labeled with DBCO-AF488 and lysed overnight with mutanolysine, lysozyme and various concentration of recombinant LytA. Lysates were centrifuged at 20,000 g for 2 min. The pellets were resuspended in one-fourth the initial volume and samples were analyzed by gel electrophoresis. Fluorescently labeled compounds were revealed by UV trans-illumination.

Notes on the electrophoresis

Several points should be made regarding the electrophoretic system. We used gels with acrylamide concentrations of either 12% or 17%. Although the acrylamide concentration had little consequence on the separation of WTA and LTA, we observed that the migration of small soluble compounds was greatly affected (SI **Figs S7A-B**). Thus, the phospho-choline-triazole-AF488 migrates a lesser distance than the choline-triazole-AF488 or the DBCO-AF488 in 12% acrylamide gels, whereas the opposite occurs in 17% gels. The separation of the choline-triazole-AF488 and the DBCO-AF488 is not sufficient in 17% gels.

Also, we found that thiol reducing agents such as DTT routinely included when loading the gels do react with DBCO-AF488 to yield a mixture of species, denoted with * in SI **Figs S7A-B**. The extent of this reaction appeared to depend on the length and conditions of the storage of the samples prior to analysis and therefore was not controlled.

In some cases, such as in **Figs 6A, 6B or 6E**, one or multiple additional weak but sharp bands of fluorescently labeled material appear on the gels above the LTA bands. These bands can be correlated to Coomassie-stained protein bands (SI **Figs S8D-F**) and they are likely products of the reaction of DBCO-AF488 with protein thiols or primary amines. As stated above for the modification of DBCO-AF488, this side reaction was not controlled and not always present. A weak non-specific fluorescent labeling of cellular proteins by DBCO-AF488, which was not a problem when TA were labeled during the whole culture, contributed to a significant smear bluring the TA bands when labeling was performed only during a short pulse time such as in **Fig. 5C**.

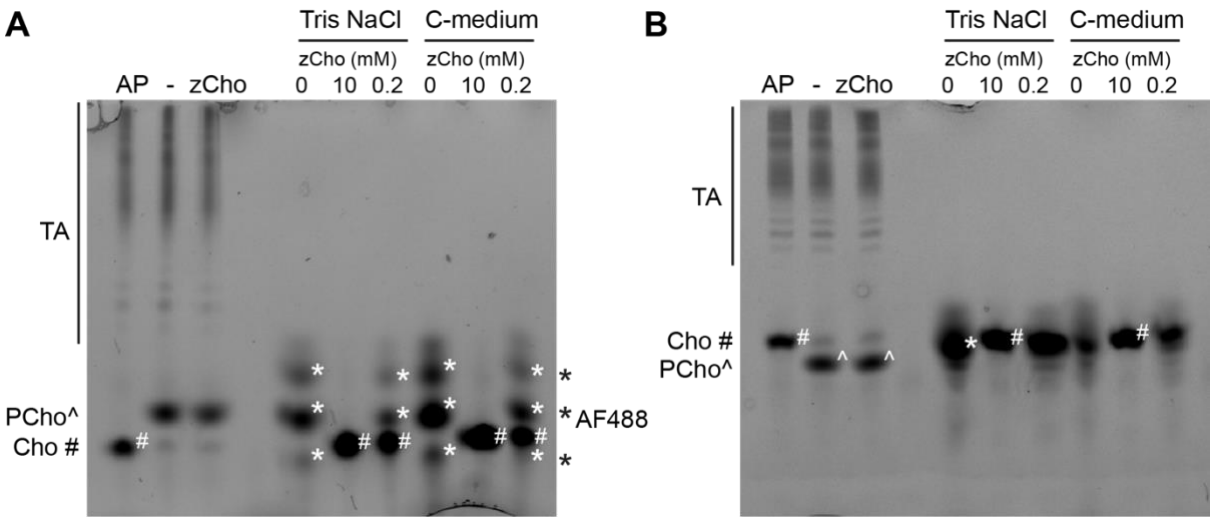

Figure S7. Polyacrylamide gel electrophoresis of click-labeled TA, azido-choline (zCho) and the clickable fluorophore DBCO-AF488 with (**A**) 12% (w/v) and (**B**) 17% acrylamide. Three lanes on the left of the gels: R800 cells were grown in C-medium in the presence of 0.2 µM azido-choline prior to lysis and secondary labeling with 10 µM DBCO-AF488 overnight at room temperature. Samples were further incubated 4 h with either 1000 $U.mL^{-1}$ alkaline phosphatase (AP), nothing (-), or 10 mM additional azido-choline. Six lanes on the right of gels. In either 50 mM Tris pH 8, 150 mM NaCl or C-medium, 20 µM DBCO-AF488 were incubated at room temperature for 4 h with either 0, 10 mM or 200 µM azido-choline. Prior to gel loading, samples were supplemented with 8% glycerol, 0.8% SDS, 8 mM DTT and trace of bromophenol blue. The migration position of the fluorophore-triazole-linked species are indicated on the left or on the gels by symbols (PCho^, phospho-choline; Cho*, choline). The position of the DBCO-AF488 reagent is indicated on the right or on the gel with the symbol #.

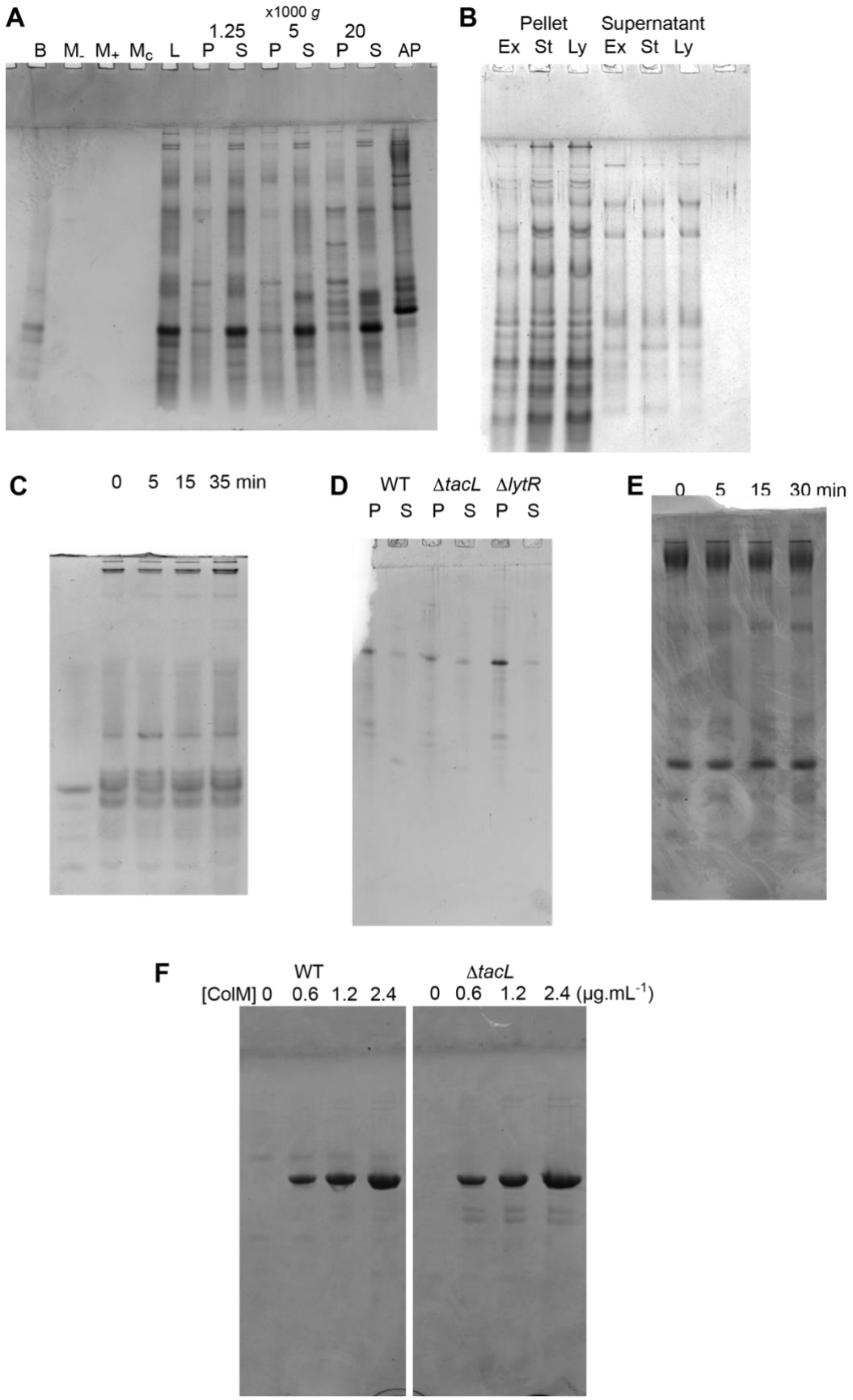

Figure S8. Protein Coomassie staining of TA analysis gels presented in Figs 4A, 5A, 5B, 6A, 6B, 6E.

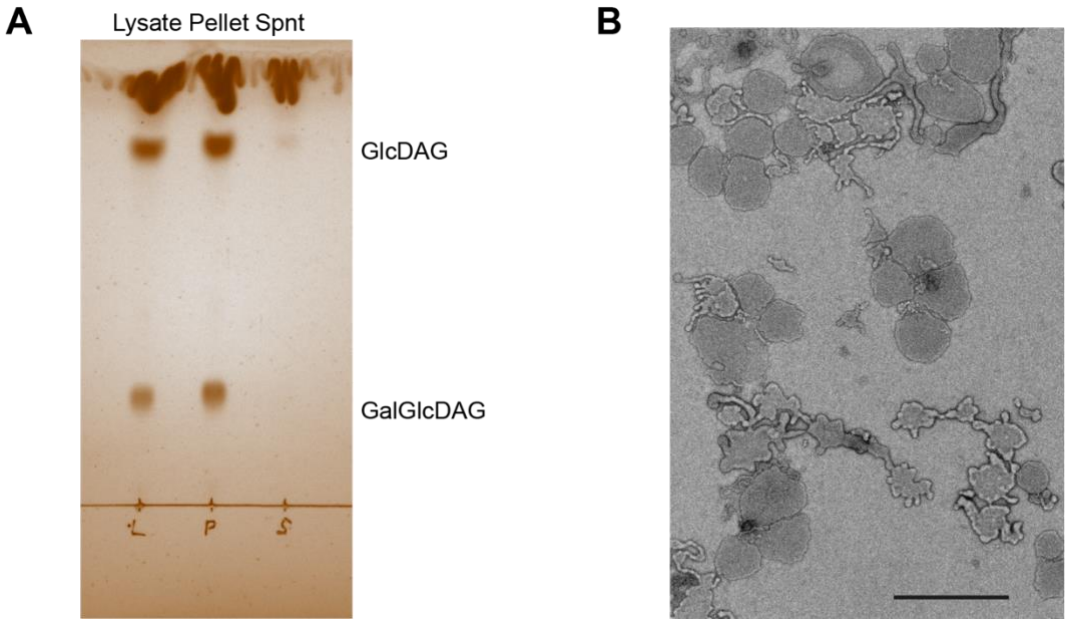

Figure S9. Characterization of the cell lysate fractionation by sedimentation. (**A**) Iodine vapor-stained thin layer chromatography of lipids extracted from R800 cell lysate, the resuspended low-speed centrifugation pellet and the supernatant (Spnt) of the lysate. Lipids were tentatively identified according (2). GlcDAG, mono-glucosyl-diacyl-glycerol (DGlc*p*-DAG); GalGlcDAG, galactosyl-glucosyl-diacyl-glycerol (DGal*p*-DGlc*p*-DAG). (**B**) Negative stain electron micrograph of the resuspended low-speed centrifugation pellet. Magnification was 4800x. Scale bar is 1 µm.

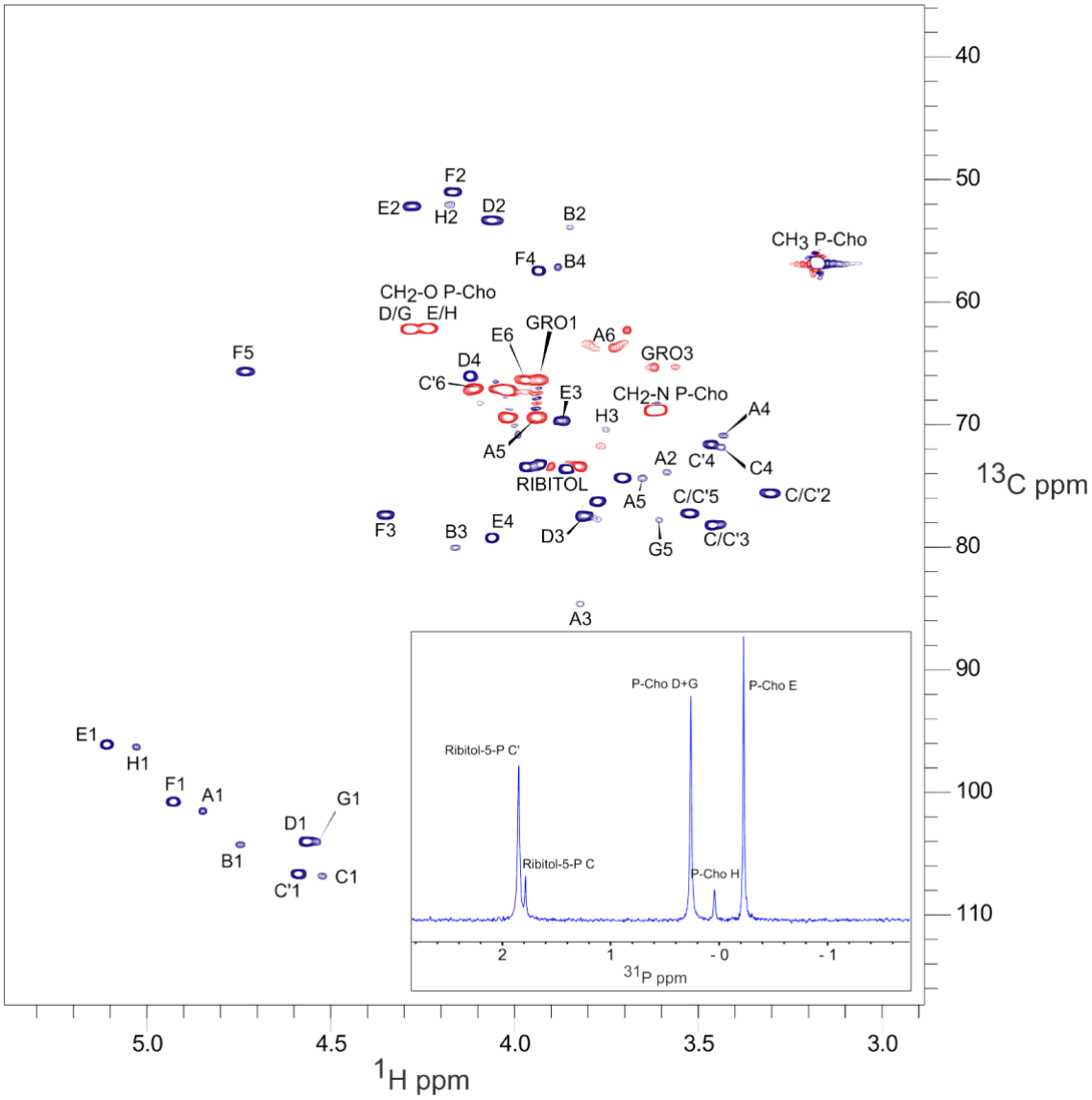

Figure S10. NMR spectra of *S. pneumoniae* LTA obtained by low speed centrifugation of cell lysate. Main is ^{13}C-^{1}H HSQC (constant-time) spectrum; ^{13}C nuclei that are coupled to either zero or two other carbons (red) and those coupled to one or three other carbons (dark blue), exhibit opposite signs. Inset is ^{31}P 1D spectrum. The peak nomenclature is that proposed by Gisch et al. (1). Peaks A1 to A6, GRO1 GRO3 are originating from the lipid anchor DGlc*p*-DAG of LTA.

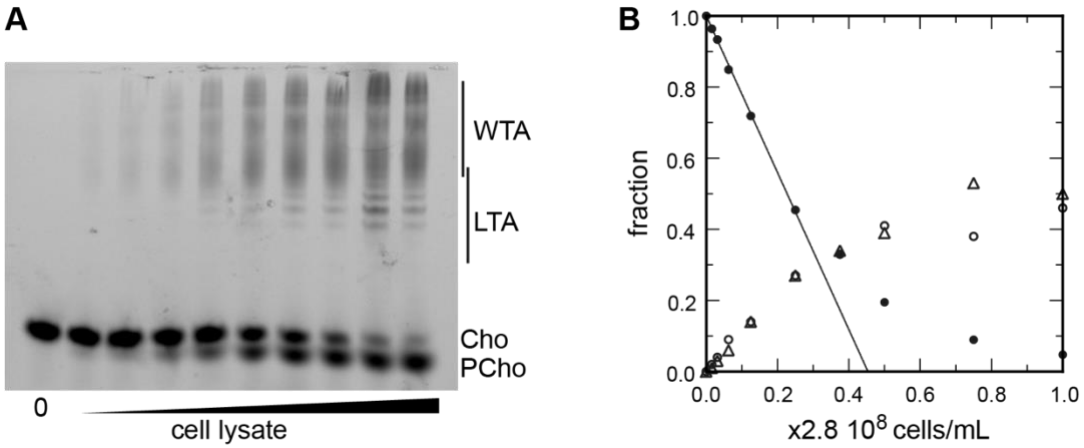

Figure S11. (**A-B**) Titration of cellular TA. R800 cells were grown for two generation in the presence of azido-choline. DBCO-AF488 (3.7 µM) was incubated for 24 h with varying amount of cell lysate corresponding to up to 2.9 10^8 cells mL^{-1}. The remaining DBCO-AF488 was blocked by addition of 100 mM azido-choline, and the various species were separated by polyacrylamide gel electrophoresis. (**A**) The gel was imaged by trans-illumination with UV light. (**B**) The bands were quantified and the relative amount of the various species were plotted against the cell concentration. Black circles, blocked DBCO-AF488; open circle, phospho-choline; open triangle, TA. A linear regression of the DBCO-AF488 points at low cellular concentration was applied to obtain the titration point as the intercept of the cell concentration axis.

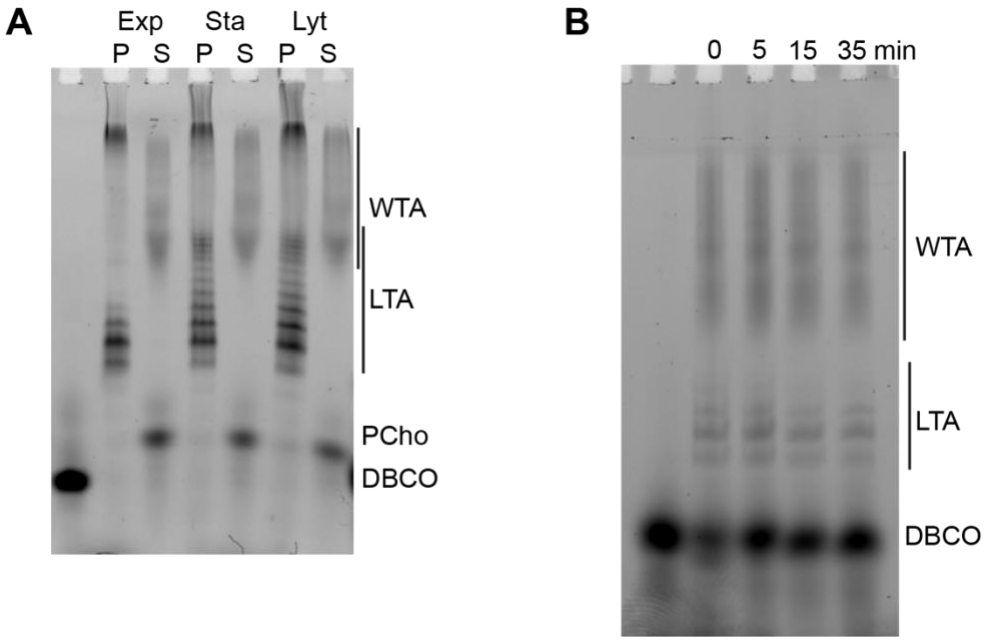

Figure S12. Evolution of TA during growth. (**A**) Δ*lytA* cells grown in C-medium containing 200 µM azido-choline were harvested during the exponential growth phase (Ex), at the onset of the stationary phase (St) and during the autolysis (Ly). TA were fluorescently click-labeled with DBCO-AF488 and cells were completely lysed by the addition of peptidoglycan hydrolases prior to centrifugation. LTA are found in the pellet (P) whereas WTA are observed in the supernatant (S). The amounts of cells at the different culture stages were normalized. The LTA samples are 8-fold concentrated compared to the WTA samples. Fluorescently labeled TA were revealed by UV-transillumination after SDS-polyacrylamide electrophoresis. (**B**) Electrophoretic analysis of TA of WT cells grown in C-medium supplemented with 0.1% yeast extract and pulse-labeled for 5 min with the addition of 0.2 mM azido-choline, and chased by further growth in the same medium without added azido-choline for the indicated duration.

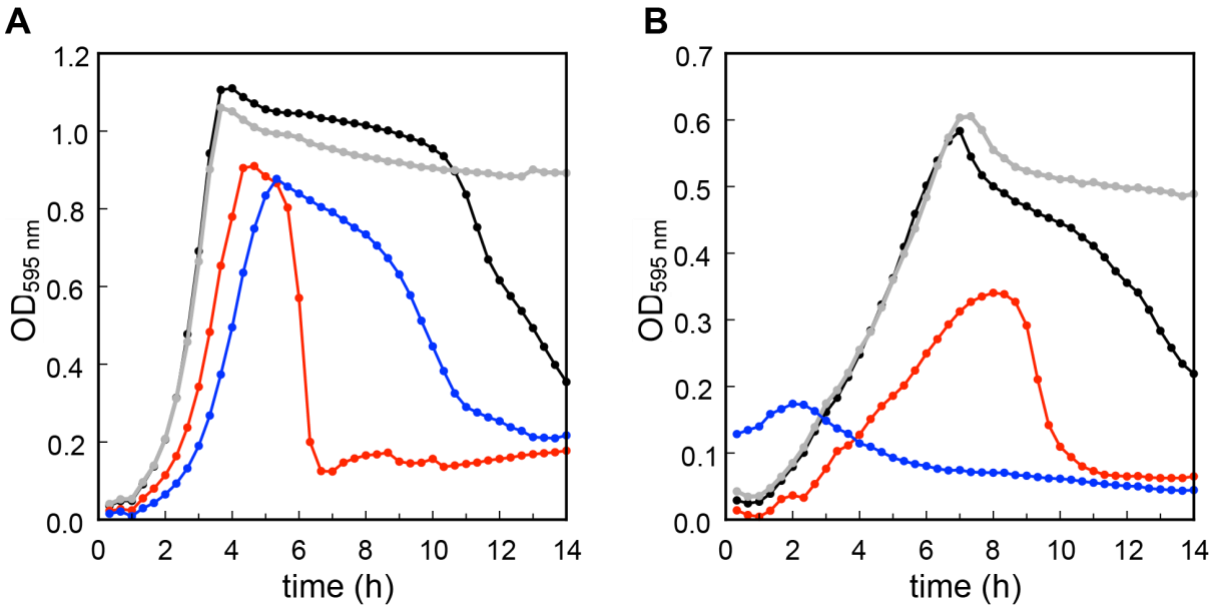

Figure S13. Growth of the *S. pneumoniae* WT (black), Δ*lytA* (gray), Δ*tacL* (red) and Δ*lytR* (blue) strains in BHI (**A**) and C-medium 200 µM choline (**B**).

Discussion of the sedimentation of *S. pneumoniae* LTA

Finally, a technical point requires discussion. The use of fluorescent labeling allowed to track the TA during cell fractionnation and revealed that membranes from *S. pneumoniae* sediment at low relative centrigugal force (**Fig. 4A**). This was a surprise to us, since we were used, as many other laboratories, to pellet membranes from *E. coli* for the preparation of recombinant proteins at 100,000 *g* after a clarification step at 40,000 *g*. However, considering the membrane composition could have predicted this outcome. The sedimentation coefficient *s* is proportional to $1 - \rho\bar{v}$ were ρ is the density of the solvent (close to 1 for aqueous biochemical solutions) and $\bar{v}$ is the partial-specific volume of the particle (the reciprocal of the density). For a complex particle such a membrane, $\bar{v}$ is the weighted sum of its components $\bar{v} = \sum_i^n w_i \bar{v}_i$. In *E. coli*, glycolipids are absent of the plasma membrane, which consists mostly of phosphatidylethanolamine (~78%), phosphatidylglycerol (~12%) and cardiolipin (~6%) (3). The partial-specific volume $\bar{v}_i$ of the various phospholipids is comprised between 0.93 and 1 (4), so that the partial-specific volume $\bar{v}$ of the *E. coli* membrane is also close to 1 and its sedimentation coefficient *s* is very small. In *S. pneumoniae* in contrast, the glycolipids mono-glucosyl-diacylglycerol (~35%) and galactosyl-glucosyl-diacylglycerol (~45%) are the major constituent of the membrane, with minor contributions of phosphatidylglycerol (~13%) and cardiolipin (5). Since the partial-specific volume $\bar{v}_i$ of glucose and galactose is 0.622 (4) and 80% of the pneumococcal lipids carry one or two hexoses, the resulting partial-specific volume $\bar{v}$ of the membrane should be around 0.8, and consequently the membranes of *S. pneumoniae* have a larger sedimentation coefficient s than those of *E. coli*. Note that the LTA themselves further increase the sedimentation coefficeint by contributing additional saccharidic units to the membrane composition.

References

1. N. Gisch, *et al.*, Structural reevaluation of Streptococcus pneumoniae Lipoteichoic acid and new insights into its immunostimulatory potency. *J. Biol. Chem.* **288**, 15654–15667 (2013).

2. M. Meiers, *et al.*, Altered lipid composition in Streptococcus pneumoniae cpoA mutants. *BMC Microbiol.* **14**, 12 (2014).

3. C. R. Raetz, Molecular genetics of membrane phospholipid synthesis. *Annu. Rev. Genet.* **20**, 253–295 (1986).

4. P. Schuck, H. Zhao, C. A. Brautigam, R. Ghirlando, *Basic principles of analytical ultracentrifugation* (CRC Press, 2016).

5. P. Calvez, J. Jouhet, V. Vié, C. Durmort, A. Zapun, Lipid Phases and Cell Geometry During the Cell Cycle of Streptococcus pneumoniae. *Front. Microbiol.* **10** (2019).